Coordination Chemistry Reviews 254 (2010) 765–780

Contents lists available at ScienceDirect

Coordination Chemistry Reviews

journal homepage: www.elsevier.com/locate/ccr

Review

Cationic organoiron mixed-sandwich hydrazine complexes: Reactivity toward aldehydes, ketones, β-diketones and dioxomolybdenum complexes

Carolina Manzur[a], Mauricio Fuentealba[a,1], Jean-René Hamon[b,*], David Carrillo[a,**]

[a] Laboratorio de Química Inorgánica, Instituto de Química, Pontificia Universidad Católica de Valparaíso, Valparaíso, Chile
[b] UMR 6226 Sciences Chimiques de Rennes, CNRS-Université de Rennes 1, Campus de Beaulieu, 35042 Rennes Cedex, France

Contents

ARTICLE INFO

Article history:
Received 26 August 2009
Accepted 2 November 2009
Available online 11 November 2009

Keywords:
Organometallic hydrazines
Organometallic hydrazones
Organometallic pyrazoles
Organometallic diazenido complexes
Nonlinear optics
Charge-transfer hybrids

ABSTRACT

This review covers comprehensively the authors work during the present decade based on the chemistry of ionic organometallic hydrazines formulated as $[(\eta^5\text{-Cp}')\text{Fe}(\eta^6\text{-Ar-NHNH}_2)]^+\text{PF}_6^-$ ($\text{Cp}' = \text{C}_5\text{H}_5$, C_5Me_5; Ar = aryl), that could be considered as a new generation of hydrazines owing to the changes provoked by the coordination of the 12-electron $\text{Cp}'\text{Fe}^+$ fragment both in the electronic properties of the aromatic ring and in the hydrazine group. The reactivity of this new class of hydrazine is obviously centered, as in the classic Fischer's organohydrazines, Ar-NHNH_2, on the $-\text{NHNH}_2$ functional unit which is able to react with aldehydes, RCH(=O) (R = alkyl, aryl, ferrocenyl (Fc)) and ketones, RR′C=O (R = alkyl, aryl; R′ = alkyl, aryl, Fc), to afford ionic organometallic hydrazones. Likewise, the mixed-sandwich hydrazine precursors react with β-diketones Me–C(=O)–CH_2–C(=O)–Me to afford ionic organometallic pyrazoles, and with *cis*-dioxo-molybdenum complexes, *e.g.* $[\text{MoO}_2(\text{S}_2\text{CNEt}_2)_2]$, to afford ionic organometallic mono-organodiazenido complexes in which the two metal centers are connected by a $\mu,\eta^6{:}\eta^1$-aryldiazenido bridge. While some ionic hydrazones exhibit NLO properties, the ionic organodiazenido hybrid complexes exhibit charge-transfer features.

* Corresponding author. Tel.: +33 02 23 23 59 58; fax: +33 02 23 23 56 37.
** Corresponding author. Tel.: +56 32 227 49 14; fax: +56 32 227 49 39.
E-mail addresses: jean-rene.hamon@univ-rennes1.fr (J.-R. Hamon), david.carrillo@ucv.cl (D. Carrillo).
[1] Present address: Departamento de Ciencias Químicas. Universidad Nacional Andrés Bello, Santiago, Chile.

0010-8545/$ – see front matter © 2009 Elsevier B.V. All rights reserved.
doi:10.1016/j.ccr.2009.11.001

1. Introduction

The study of substituted organic hydrazines can be traced back to 1875s with the first synthesis and characterization of phenylhydrazine (C_6H_5-$NHNH_2$) [1], by Emil Fischer, who was awarded the Nobel Prize for Chemistry in 1902 [2]. Since then, a large number of contributions on the synthesis, reactivity and applications of new members of this important family of aromatic dinitrogen-containing compounds has appeared. As a result, the synthesis of hydrazones, osazones, indoles, pyrazoles, thiosemicarbazides, pyridazines, etc., are well known in organic chemistry, and publications account for this spectacular development [3,4]. Likewise, over the last four decades, extensive research has also been performed on reactions of hydrazine or substituted hydrazines with transition-metal complexes, particularly the complexes of early or middle transition metals for which various coordination modes are observed (Fig. 1A–C) [5], to elucidate how the nitrogen–nitrogen bond is cleaved by a transition-metal complex [6–11]. For this purpose, chemists have synthesized and characterized a large number of organodinitrogen transition-metal complexes containing diazene (HNNH) [12–14], diazenido (NNR), hydrazido(2-) (NNRR′) and hydrazido(1-) (NHNRR′) [15–31] ligands, which have been considered as probable intermediate species in the mechanism of the enzymatic or industrial N_2 to NH_3 conversion [32–35]. Those ligands are closely related to hydrazine coordinated to transition-metal-assisted nitrogen–nitrogen bond cleavage. This chemistry of model coordination compounds with the prospect of catalytically converting dinitrogen to ammonia at room temperature and ambient pressure, such as in biological nitrogen fixation systems, still remains a real challenge, but these results fall outside the scope of this review and are regularly discussed in the literature [36–45].

On the other hand, π-complexation of aromatics to electron-withdrawing transition-metal moieties such as tricarbonylchromium, tricarbonylmanganese, cyclopentadienyliron/ruthenium and pentamethylcyclopentadienyliron/ruthenium subunits, alters their chemical reactivity and provides a variety of synthetically useful organic transformations through nucleophilic additions/substitutions, and benzylic deprotonation, affording functionalized ligands which can then be conveniently recovered as free arenes upon thermal, photochemical, oxidative or reductive removal of the metal [46–53]. In this respect, the synthesis of organometallic hydrazines where the phenyl group of a classic aromatic hydrazine is linked to the iron atom of a 12-electron cationic $[(\eta^5\text{-Cp}')Fe]^+$ arenophile, Cp′ = C_5H_5 (Cp) or C_5Me_5 (Cp*), in a hexahapto fashion (Fig. 1D), represents an exceptional opportunity to

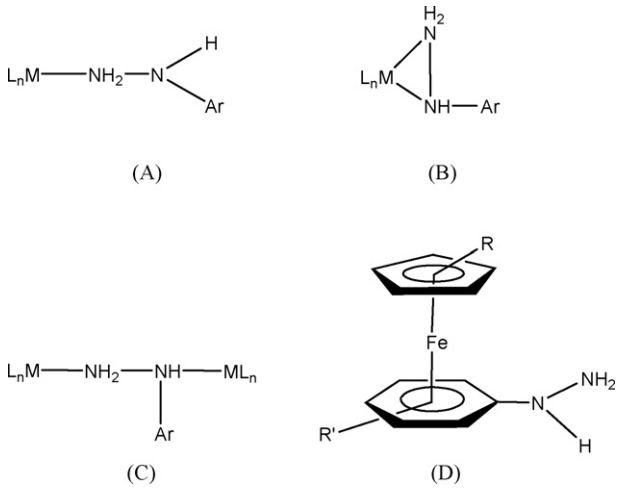

Fig. 1. Possible bonding modes of arylhydrazine to transition metals.

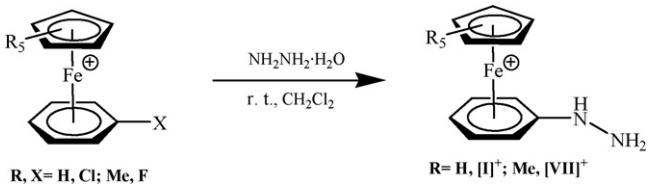

Scheme 1. Preparation of the cationic organometallic hydrazines [**I**]$^+$–[**VII**]$^+$.

re-create, in the field of coordination chemistry, the chemistry of this important class of compounds. This comprehensive review surveys the work that we have carried out during the present decade based on arylhydrazine cyclopentadienyliron complexes. We will begin with the preparation, spectroscopic and structural properties of this new class of ionic mixed-sandwich derivatives (Section 2), followed by the synthesis and physico-chemical properties of their derivatized organometallic hydrazone (Section 3) and pyrazole (Section 4) counterparts, while Section 5 will deal with organometallic–inorganic diazenido hybrid complexes resulting from reactions between organoiron hydrazine precursors and *cis*-dioxo molybdenum species.

2. Organometallic hydrazines

2.1. Synthesis

The first cationic organometallic hydrazine, formulated as $[(\eta^5\text{-Cp})Fe(\eta^6\text{-}RC_6H_4\text{-}NHNH_2)]^+$ (R = H [**I**]$^+$) was prepared as its picrate salt in 1982 by Neto and Miller [54]. This explosive and light-sensitive compound was subsequently and conveniently converted to its much safer tetrafluoroborate counterpart. Later, other members of this new family were reported, particularly those where R = 4-Me [**II**]$^+$ [55]; 2-Cl [**III**]$^+$ [56]; 3-Me [**IV**]$^+$ [57,58]; 4-MeO [**V**]$^+$ [57,58]; 4-Cl [**VI**]$^+$ [59]. In 2007, our group reported a new organometallic hydrazine, the pentamethylated analogue of the parent [**I**]$^+$, formulated as $[(\eta^5\text{-Cp}^*)Fe(\eta^6\text{-}C_6H_5\text{-}NHNH_2)]^+$ [**VII**]$^+$ [60]. The cationic organometallic hydrazines [**I**]$^+$–[**VI**]$^+$ are readily prepared by $[(\eta^5\text{-Cp})Fe]^+$-induced nucleophilic aromatic substitution [50–53] of the chloroarene of the corresponding starting material $[(\eta^5\text{-Cp})Fe(\eta^6\text{-R-}C_6H_4\text{-Cl})]^+$ with hydrazine hydrate, $NH_2NH_2{\cdot}H_2O$ (Scheme 1). The synthesis of [**VII**]$^+$ required the use of the fluorine atom as the arene substituent in the complex $[(\eta^5\text{-Cp}^*)Fe(\eta^6\text{-}C_6H_5\text{-F})]^+$ [60,61], in which this halogen is a better leaving group than chlorine in $[(\eta^5\text{-Cp}^*)Fe(\eta^6\text{-}C_6H_5\text{-Cl})]^+$, in order to compensate the decreased positive charge on the arene ligand in the Cp* series compared to the Cp series. While the synthesis of [**I**]$^+$ was carried out in EtOH, those of [**II**]$^+$–[**VII**]$^+$ were accomplished in dichloromethane (CH_2Cl_2). From the experimental point of view, the best conditions established in our laboratories in order to reach the highest yields have been: (i) the use of a hydrazine hydrate/precursor molar ratio of 6–12:1 and (ii) a reaction time of 15 h at room temperature. These complexes have indeed been synthesized under extremely mild conditions and isolated as their hexafluorophosphate (PF_6^-) salts as yellow-orange photosensitive, though air and thermally stable, microcrystalline solids in yields ranging from 26 to 66%.

2.2. Spectroscopy

The spectroscopic properties of the organometallic hydrazines discussed here are very similar to one another. Indeed, the solid (KBr) IR spectra of compounds **I**–**VII** exhibit two broad weak to medium absorption bands at *ca.* 3416–3444 and 3374–3383 cm^{-1} assigned to the stretching mode of the N–H bond and to the overlapped asymmetric and symmetric stretching modes of the

terminal NH_2 group, respectively. Likewise, at 1554–1560 cm^{-1} a sharp medium to strong band corresponding to the deformation mode of the NH_2 group was also observed. In addition, the two characteristic intense vibration modes of the PF_6^- anion appeared at 840–830 and 558 cm^{-1}, respectively.

The ^1H NMR spectra, recorded in acetone-d_6 at 297 K, show singlets at *ca.* 5.0 ppm for the cyclopentadienyl protons of the cationic organometallic hydrazines [**I**]$^+$–[**VI**]$^+$ and at 1.97 ppm for the methyl protons of the η^5-Cp* ligand of [**VII**]$^+$, indicating that each nucleophilic substitution reaction leads to a unique product. In the seven cases, the –NH–NH_2 protons exhibit two resonances in the integral signal ratio 2:1 at 2.96–3.04, 8.60–8.89 ppm ranges and 4.44, 7.35 ppm for [**I**]$^+$–[**VI**]$^+$ and [**VII**]$^+$, respectively. The high field resonances are attributed to the NH_2 protons, while the low field ones correspond to the benzylic NH protons due to the electron-withdrawing properties of the [(η^5-Cp′)Fe]$^+$ cationic moiety linked to the phenyl ring. The NH signal of [**VII**]$^+$ is upfield shifted by 1.40–1.44 ppm compared to those of its Cp counterparts, thus, nicely illustrating the increased electronic density onto the arene ring upon coordination to the [(η^5-Cp*)Fe]$^+$ arenophile. In the $^{13}C\{^1H\}$ NMR spectra, besides all the expected peaks, the arene carbons bearing the –NH–NH_2 group resonate in the range 110–120 ppm as slightly broadened signals.

2.3. X-ray molecular structures

The molecular structure of the parent organometallic hydrazine **I** [58] and its pentamethylated derivative **VII** [60] have been determined by single crystal X-ray diffraction analysis. For the sake of comparison, the ball-and-stick views of the two cationic organometallic moieties [**I**]$^+$ and [**VII**]$^+$ are presented in Fig. 2 in similar perspectives. Both compounds display the classical sandwich structure of the type [(cyclopentadienyl)iron(arene)]$^+$ cation, adopting the [η^5-Fe-η^6]$^+$ metallocene-type coordination mode, with Fe–Cp and Fe-arene centroid distances of 1.668, 1.552 Å and 1.665, 1.555 Å for [**I**]$^+$ and [**VII**]$^+$, respectively. The two carbocyclic rings are essentially parallel with one another, with in both cases, a ring centroid-iron-ring centroid angle of 179.4° [62]. However, the distances between the iron center and the arene carbon bearing the –NH–NH_2 group are 0.071 and 0.112 Å longer than the mean value of the other Fe–C bond lengths. This elongation is a consequence of a partial delocalization of the benzylic nitrogen electron lone-pair toward the cationic mixed-sandwich moiety, and is reflected by (i) a depyramidalization with idealized bond angles at this sp^2-hybridized nitrogen atom of 119.0(8)° and 118.1(2)°, (ii) a carbon–nitrogen bond distances of 1.333(9) and 1.367(4) Å, which are intermediate between a single and double carbon–nitrogen bond [63], and (iii) a weak cyclohexadienyl-like character of the coordinated phenyl ring with a folding dihedral angle of 6.0° and 7.4° between the plane containing the C–N vector and that of the remaining pentadienyl framework. The substitution of the bulky electron rich [(η^5-Cp)Fe]$^+$ arenophile for its parent [(η^5-Cp*)Fe]$^+$ counterpart has virtually no effect on the deformation of the phenylhydrazine ligand toward an iminocyclohexadienyl structure. The distortions of the arene ligand in hexahapto coordinated arene complexes are, indeed, mainly influenced by the electronegativity, the inductive and the resonance effects of the arene substituents rather than by the nature of the 12-electron coordinating organometallic [ML_n]$^{0/+}$ moiety [64–67].

3. Organometallic hydrazones

Hydrazones [68] have been intensively investigated mostly because of their potential applications as anticancer, antiviral, antibacterial, and antifungal agents [69,70]. These compounds display a versatile behavior in metal coordination, and their biological activity is often increased by bonding to transition metals [71]. On the other hand, hydrazones have been extensively used by Enders et al. in asymmetric synthesis of chiral organic and ferrocenyl ketones [72,73]. In addition, due to their chelating behavior, hydrazones are employed as ligands in metal-catalyzed allylic substitutions and cross-coupling reactions [74–77]. As well, organometallic hydrazones are a versatile class of compounds with several applications. A plethora of such compounds can be found in the literature and, therefore, we will just mention here four main categories, supported by few recent references to introduce the reader to this subject matter. Those are ferrocenylhydrazones resulting from condensation of substituted hydrazines with formyl- and acetylferrocenes, Fc–C(R)=N–NHR′, where R is H or Me, and R′ is alkyl, aryl, heterocycles or ferrocenoyl [78–81]; organometallic hydrazones of the type L_nM–N(R)–N=CR'_2 (M = transition metals, lanthanides and actinides) formed by insertion of diazoalkanes into metal–hydrogen or metal–carbon bonds [82–84]; compounds containing the organometallic hydrazone core [M–CH_2C(R)=N–NMe_2] (M = Al, Zn) [85–87]; and cyclopalladated derivatives where the hydrazone ligand is linked to the metal center through an *ortho*-carbon of a phenyl substituent and a heteroatom of the hydrazone backbone [88,89]. The first hexahapto coordinated organometallic hydrazones, formulated as (η^6-2-R–C_6H_4–CH=N–NMe_2)$Cr(CO)_3$ (R = H, Me, *n*-Bu), were reported by Kündig et al. [90]. In such complexes, the hydrazone functionality is attached to the arenetricarbonylchromium fragment through the azomethine carbon atom.

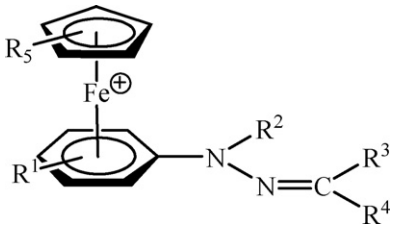

Chart 1.

Interestingly, hydrazones that contain the asymmetric transmitter backbone –NHN=CR– allow, for a given electron-donating (D) and electron-withdrawing (A) group, the formation of two different types of compounds: A-NHN=CR-D (Type I) and D-NHN=CR-A (Type II) [91,92]. Particularly, Type I hydrazones containing the 4-nitrophenyl group as acceptor and 4-dimethylaminophenyl, 4-methoxophenyl, 4-bromophenyl or 4-methylphenyl groups as donors have shown efficient second-order nonlinear activity [91]. Knowing that the chlorine atom of the chlorobenzene cyclopentadienyliron complex has a mobility comparable to 2,4-dinitrochlorobenzene [51,53], it was tempting to explore an expansion of the important push–pull hydrazone structure into the third dimension. This can in principle be done by formally attaching the electron-withdrawing [(η^5-Cp′)]$^+$ moiety to one arene of the planar framework by the 3D extension of the mixed-sandwich unit. Thus, using the organometallic hydrazines depicted in Section 2, we have replaced one two-dimensional carbocyclic ring by an electronically related three-dimensional electron-withdrawing robust metallocene system. Peculiar electronic and structural properties were, of course, observed for this new family of ionic organometallic hydrazones derivatives.

3.1. Synthesis

Chart 1 shows a representative backbone of the sixty-six different organometallic hydrazones that before we have prepared.

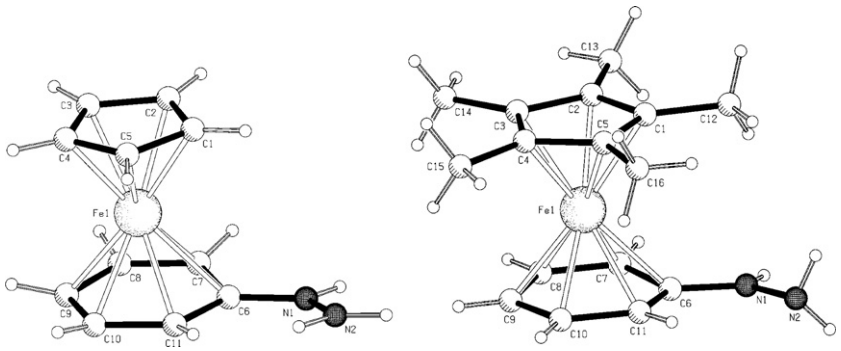

Fig. 2. Ball-and-stick views of $[(\eta^5\text{-Cp})Fe(\eta^6\text{-}C_6H_5\text{-}NHNH_2)]^+$ [**I**]$^+$ (left [58]) and $[(\eta^5\text{-Cp}^*)Fe(\eta^6\text{-}C_6H_5\text{-}NHNH_2)]^+$ [**VII**]$^+$ (right [60]). PF_6^- counterions have been omitted for clarity.

They are gathered in Table 1 [57–60,93–102]. Each mononuclear (**VIII**–**XLIII**), binuclear (**XLIV**–**LXVII**) and trinuclear (**LXVIII**–**LXXIII**) organometallic hydrazone is depicted according to the nature of the R, R^1, R^2, R^3 and R^4 substituents. The syntheses of these new organometallic hydrazones have been carried out by direct condensation reaction of the corresponding organometallic hydrazines with different organic or organometallic aldehydes or ketones in refluxing ethanol, under inert atmosphere (N_2). Some drops of glacial acetic acid or, in some cases, hexafluorophosphoric acid was added as the catalyst. The hydrazones were always isolated as orange, yellow, red, yellow-orange or reddish-orange crystalline solids giving directly or by recrystallization in CH_2Cl_2, acetonitrile or a mixture of both solvents, suitable single crystals for X-ray diffraction studies. In some cases, the formation of single crystals was favored by slow diffusion of layered diethyl ether in those solutions.

3.2. Spectroscopy

Let's first introduce the characteristic IR bands and NMR signals that could be considered as probes in the rapid identification of this type of organometallic hydrazones. Indeed, the most important features invariably exhibited by the solid (KBr) IR spectra [103] of this family of organometallic hydrazones, associated with the formation of the –NHN=C(R^3)– functionality, are: (i) the presence of only the medium and sharp stretching bands corresponding to the N–H group, in the 3392–3289 cm^{-1} region, and (ii) the appearance of characteristic sharp intense stretching band in the C=N imine group in the 1574–1525 cm^{-1} region. As for their organometallic hydrazine precursors, the PF_6^- counter anion is easily identified by its typical very strong $\nu(PF_6)$ and strong δ(P–F) bands observed in the 860–825 and 559–554 cm^{-1} regions, respectively. On the other hand, depending on the crystallinity of the samples, some bands give rise to two stretching vibrations. For example, the IR spectrum of a crystalline sample of [**XLVIII**] shows two N–H stretching frequencies at 3368 and 3322 cm^{-1}, whereas only one N–H absorption at 3344 cm^{-1} is observed in solution at room temperature. The dynamic behavior of this compound was confirmed by variable-temperature NMR experiments which allow the determination of two similar activation energies ($\Delta G^{\#}$ = 41 kJ/mol) for the hindered rotation of the cationic mixed sandwich $[(\eta^5\text{-Cp})Fe(\eta^6\text{-}C_6H_5)]^+$ around the C_{phenyl}–N bond and of the ferrocenyl fragment around the its C_5H_4–C linkage to the hydrazone core [59]. These observations are compatible with the presence of both *syn* and *anti*-rotamers in the crystalline form, as it was revealed later on by the X-ray crystal structure analysis (see Section 3.4). Likewise, the solid IR spectra of the homotrimetallic compounds **LXVIII**–**LXXI** show the splitting of the ν(N=C), $\nu(PF_6)$ and ν(C–Cl), in the case of [**LXIX**] [101], suggesting the presence of at least two conformers in the solid state.

On the other hand, all the organoiron hydrazones listed in Table 1 are stereoselectively formed at the sterically less hindered *trans*-isomer about the N=C double bond, as indicated by the unique set of signals in their ^{1}H and ^{13}C NMR spectra for which the stereochemistry and assignments were performed with the aid of NOE experiments and 2D homo- and heteronuclear correlation spectroscopy, respectively. For instance, the Cp and Cp* protons of the sandwich moiety $[(\eta^5\text{-Cp}')Fe(\eta^6\text{-R-}C_6H_4)]^+$ resonate as sharp singlets at 5.11–5.24 and 1.93–1.98 ppm, respectively, the former signals being slightly downfield shifted compared to those of their corresponding hydrazine precursors. In the case of bi- and trinuclear hydrazones capped with a terminal 1-ferrocenyl subunit, the Cp proton resonances of the unsubstituted ring are observed as sharp singlets in the 4.03–4.43 ppm range. The hydrazonedyil spacer –NH–N=CH– is clearly identified by the low field azomethine N=CH and acidic benzylic N–H [94] protons which show up as slightly broadened peaks at 7.80–8.60 ppm, respectively. The latter resonances are again ostensibly downfield shifted compared to the N–H signals in their hydrazine counterpart, indicating depyramidalization of the nitrogen atom with a greater partial delocalization of the positive charge along the conjugated hydrazone backbone and concomitant cyclohexadienyl character at the coordinated C_6-ring. Note that the highest value (δN–H = 10.20) is observed for the dicationic derivative [**LXVII**]$^{2+}$ where a second acceptor fragment ($[(\eta^5\text{-Cp}^*)Ru]^+$) is present in the molecule [60]. In addition, the low field position of the acidic benzylic NH signal may also be attributed to its participation in various types of hydrogen bonding (see Section 3.5). Finally, for the series of binuclear hydrazones **LII**–**LV**, a very good correlation is obtained with ^{1}H NMR chemical shifts of the benzylic N–H proton resonances (Fig. 3), using the classic Hammett σ_p set of parameters [68,104] (Eq. (1); R = 0.997). The positive slope indicates that electron-withdrawing substituents induce a marked deshielding of the corresponding ^{1}H NMR shift. The more electron-withdrawing the 4-R^1 substituent (more positive the σ_p parameter) the more shifted is the NH proton resonance [99]. Such a correlation was also reported by Nesmeyanov and co-workers for substituted $[(\eta^5\text{-Cp})Fe(\eta^6\text{-}p\text{-}XC_6H_4Me)]^+PF_6^-$ derivatives [105].

$$\delta_{N-H}(\text{ppm}) = 0.47\sigma_p + 8.90 \quad (1)$$

Besides the expected characteristic sharp singlet resonances of the Cp or Cp* ligand of the mixed sandwich $[(Cp')Fe(RC_6H_4-)]^+$, the proton decoupled ^{13}C NMR spectra of the studied organometallic hydrazones exhibit broader peaks of the two carbons linked to a nitrogen atom. The imine carbon appears at *ca.* 145 ppm and the coordinated C_{ipso} at *ca.* 120 ppm, in accordance with a multi-

Table 1
List of prepared organometallic hydrazones, isolated as their PF_6^- salts.

Compound	R	R^1	R^2	R^3	R^4	Ref.
VIII	H	H	H	Me	Me	[57,58]
IX	H	2-Cl	H	Me	Me	[57,58]
X	H	4-Me	H	Me	Me	[57,58]
XI	H	4-OMe	H	Me	Me	[57,58]
XII	H	H	H	Me	C_6H_4-4-Me	[93]
XIII	H	H	H	Me	C_6H_4-4-OMe	[93]
XIV	H	H	H	Me	C_6H_4-4-NMe_2	[93]
XV	H	2-Cl	H	Me	C_6H_4-4-Me	[93]
XVI	H	2-Cl	H	Me	C_6H_4-4-OMe	[93]
XVII	H	2-Cl	H	Me	C_6H_4-4-NMe_2	[93]
XVIII	H	2-Me	H	Me	C_6H_4-4-Me	[93]
XIX	H	2-Me	H	Me	C_6H_4-4-OMe	[93]
XX	H	2-Me	H	Me	C_6H_4-4-NMe_2	[93]
XXI	H	2-OMe	H	Me	C_6H_4-4-Me	[93]
XXII	H	2-OMe	H	Me	C_6H_4-4-OMe	[93]
XXIII	H	2-OMe	H	Me	C_6H_4-4-NMe_2	[93]
XXIV	H	H	H	H	C_6H_5	[94]
XXV	H	H	H	H	C_6H_4-4-Me	[94]
XXVI	H	H	H	H	C_6H_4-4-OMe	[94]
XXVII	H	H	H	H	C_6H_4-4-NMe_2	[94]
XXVIII	H	2-Cl	H	H	C_6H_4-4-Me	[94]
XXIX	H	2-Cl	H	H	C_6H_4-4-OMe	[94]
XXX	H	2-Cl	H	H	C_6H_4-4-NMe_2	[94]
XXXI	H	2-Me	H	H	C_6H_4-4-Me	[94]
XXXII	H	2-Me	H	H	C_6H_4-4-OMe	[94]
XXXIII	H	2-Me	H	H	C_6H_4-4-NMe_2	[94]
XXXIV	H	2-OMe	H	H	C_6H_4-4-Me	[94]
XXXV	H	2-OMe	H	H	C_6H_4-4-OMe	[94]
XXXVI	H	2-OMe	H	H	C_6H_4-4-NMe_2	[94]
XXXVII	H	H	Me	H	C_6H_4-4-Me	[94]
XXXVIII	H	H	Me	H	C_6H_4-4-OMe	[94]
XXXIX	H	H	Me	H	C_6H_4-4-NMe_2	[94,95]
XL	H	4-Me	H	H	a	[96]
XLI	H	4-Me	H	H	b	[96]
XLII	H	4-Me	H	H	c	[96]
XLIII	Me	H	H	H	2,4,6-$Me_3C_6H_2$	[60]
XLIV	H	H	H	H	Fc	[57,59]
XLV	H	4-Cl	H	H	Fc	[59]
XLVI	H	4-Me	H	H	Fc	[57,59]
XLVII	H	4-OMe	H	H	Fc	[57,59]
XLVIII	H	H	H	Me	Fc	[59]
XLIV	H	4-Me	H	Me	Fc	[59]
L	H	4-OMe	H	Me	Fc	[59]
LI	H	4-Me	H	(C_6H_4)-4-Me	Fc	[98]
LII	H	H	H	Me	CH=CH-Fc	[99]
LIII	H	4-Cl	H	Me	CH=CH-Fc	[99]
LIV	H	4-Me	H	Me	CH=CH-Fc	[99]
LV	H	4-OMe	H	Me	CH=CH-Fc	[99]
LVI	H	H	H	H	C_6H_4-4-CH=CH-Fc	[100]
LVII	H	4-Cl	H	H	C_6H_4-4-CH=CH-Fc	[100]
LVIII	H	4-Me	H	H	C_6H_4-4-CH=CH-Fc	[100]
LIX	H	4-OMe	H	H	C_6H_4-4-CH=CH-Fc	[100]
LX	H	H	H	H	Fç-CH=CH-C_6H_4-4-NO_2	[101]
LXI	H	4-Cl	H	H	Fç-CH=CH-C_6H_4-4-NO_2	[101]
LXII	H	4-Me	H	H	Fç-CH=CH-C_6H_4-4-NO_2	[101]
LXIII	H	4-OMe	H	H	Fç-CH=CH-C_6H_4-4-NO_2	[101]
LXIV	H	4-Me	H	H	Fç-CH=CH-C_6H_4-4-CN	[101]
LXV	H	4-Me	H	H	Fç-CH=CH-C_6H_4-4-Me	[101]
LXVI	Me	H	H	H	Fc	[60]
LXVII	Me	H	H	H	$\{(\eta^6\text{-}2,4,6\text{-}Me_3C_6H_2)RuCp^*\}^+$	[60]
LXVIII	H	H	H	H	Fç-CH=N-NH-$\{(\eta^6\text{-}C_6H_5)FeCp\}^+$	[101]
LXIX	H	4-Cl	H	H	Fç-CH=N-NH-$\{(\eta^6\text{-}4\text{-}ClC_6H_4)FeCp\}^+$	[101]
LXX	H	4-Me	H	H	Fç-CH=N-NH-$\{(\eta^6\text{-}4\text{-}MeC_6H_4)FeCp\}^+$	[101]
LXXI	H	4-OMe	H	H	Fç-CH=N-NH-$\{(\eta^6\text{-}4\text{-}MeOC_6H_4)FeCp\}^+$	[101]
LXXII	H	4-Me	H	H	Fç-CH=CH-Fc	[102]
LXXIII	H	4-OMe	H	H	Fç-CH=CH-Fc	[102]

Abbreviations: Cp = η^5-C_5H_5; Cp* = η^5-C_5Me_5; Fc = 1-ferrocenyl, $CpFe(\eta^5\text{-}C_5H_4)$; Fç = 1,1′-ferrocenediyl, $Fe(\eta^5\text{-}C_5H_4)_2$; a = 2,6-di-*tert*-butyl-4*H*-pyran-4-ylidene; b = (4*E*)-2-*tert*-butyl-4-*H*-chromen-4-ylidene; c = (2*Z*)-4,6-diphenyl-2*H*-pyran-2-ylidene.

ply bonded carbon–nitrogen bond. In some instances, this latter resonance splits into two peaks separated by 0.1 ppm. This could result from an equilibrium between a η^6-aminoarene and a η^5-iminocyclohexadienyl coordination modes (see Section 3.6) [106], as supported by theoretical work [107].

3.3. Linear and nonlinear optical properties

The UV–vis spectra of the majority of the organometallic hydrazones presented in Table 1, have been registered in CH_2Cl_2 (ε = 8.90) and DMSO (ε = 47.6). They display a relatively intense band,

Table 2
Bathochromic shifts as function of the acceptor strength of the appended R^4 group[a].

R^4	Fç-CH=CH-C_6H_4-4-Me (**LXV**)	Fç-CH=N-NH-{(η^6-4-MeC_6H_4)FeCp}$^+$ (**LXX**)	FçCH=CH-C_6H_4-4-CN (**LXIV**)	Fç-CH=CH-C_6H_4-4-NO_2 (**LXII**)
λ_{HEB}/nm[b]	302	309	311	321
λ_{LEB}/nm[c]	453	473	478	492

[a] Fç = 1,1′-ferrocenediyl [(η^5-C_5H_4)$_2$Fe].
[b] HEB = high-energy band.
[c] LEB = low-energy band.

involving π–π* transitions, centered between 250 and 400 nm, in addition to a less intensity feature in the longer wavelength region, responsible for the yellow to red color, and involving both the ligand and the metal center, having charge-transfer (CT) character. These CT bands exhibit a significant solvatochromism, very frequently bathochromic shifts, when the solvent polarity is increased, characteristic of a large dipole moment change between the ground and the excited state. However, in the case of the trimetallic hydrazones bearing two cationic mixed-sandwich units (**LXVIII**–**LXXI**), a negative solvatochromism, *i.e.* a hypsochromic (blue) shifts varying between −2 and −54 nm is observed with increasing solvent polarity [101], indicating a reduction in the dipole moment upon electronic excitation. The energy and intensity of the CT transitions are also influenced by the nature of the ancillary ligands. Thus, a lowering of the energy of the π* orbital of the ligand, results in bathochromic shifts in their absorption maxima [108,109]. In fact, this is what we observe in the series of the four compounds (**LXII**, **LXIV**, **LXV** and **LXX**) containing the same cationic core [(η^5-Cp)Fe(η^6-4-MeC_6H_4–NHN=CH–)]$^+$, and with R^4 substituents of various electron-accepting ability (Table 1). In this family, the two CT transitions are progressively shifted to longer wavelengths as the acceptor strength of the pendant group increases (Table 2) [101]. Similar trends have also been observed for other families of ferrocenyl p-cyanophenylethenyl and phenylethynyl compounds [110,111], as well as for cationic organoiron polymers containing azo dye-functionalized side chains [112].

The absorption bands are red-shifted with increasing the conjugated chain length between the donor and acceptor termini [99]. This is clearly illustrated in Fig. 4, by comparing the electronic spectral data of two series of binuclear organometallic hydrazones: **XLVIII**–**L** with those of **LII**, **LIV** and **LV**, respectively (Table 1). For the three former compounds the bridge consists of the methylated hydrazonediyl –NH–N=C(Me)–, while it was increased by a (*E*)–CH=CH– unit for the three latter ones. Both high- and low-energy bands are, indeed, bathochromically shifted of 2363, 4273, 1973 cm^{-1} and 1175, 2060, 2696 cm^{-1} for R^1 = H, Me, and OMe, respectively. These values are of the same magnitude as those reported for many other ferrocenyl series comprising the polyenic bridges [108,109,113], therefore, justifying the interest of our asymmetric hydrazonediyl spacer in the design of organometallic push–pull materials.

The second-order nonlinear optical (NLO) properties of hydrazone complexes derived from 2,4,6-trimethylbenzaldehyde **XLIII** and ferrocencarboxaldehyde **LXVI** [60], and those derived from the α- and γ-pyranylidenacetaldehydes, **XL**, **XLI** and **XLII** [96], have been investigated using the Electric-Field-Induced-Second-Harmonic (EFISH) generation technique at 1.91 μm. These cationic chromophores exhibit reasonable μβ values in the 80–270 × 10^{-48} esu range, although these values remain significantly weaker than those reported for extended π-conjugated organic hydrazone molecules (μβ = 100–640 × 10^{-48} esu) bearing strong acceptor nitro-phenyl end groups [114]. However, the cationic [(η^5-Cp)Fe(η^6-arene)]$^+$ moiety that can easily be functionalized owing to the [(η^5-Cp)Fe]$^+$-induced transformations at the coordinated arene ring [50–53], remains a potential interesting building block in molecular engineering of compounds with quadratic NLO properties [115].

3.4. X-ray molecular structures

Among the organometallic hydrazones listed in Table 1, the crystal structures of six mononuclear (**X**, **XXI**, **XXV**, **XXXVIII**, **XXXIX**, **XLI**), five binuclear (**XLVII**, **XLVIII**, **LI**, **LVIII**, **LXV**) and two trinuclear (**LXXI**, **LXXII**) derivatives were solved by single crystal X-ray diffraction studies. For the sake of comparison, ball-and-stick views of the cationic organometallic entity of a representative compound of each category ([**X**]$^+$, [**XLVII**]$^+$ and [**LXXII**]$^+$) with the atom-labeling schemes, are illustrated in Fig. 5. As noted above in Section 2.3 for the organometallic hydrazine precursors, the

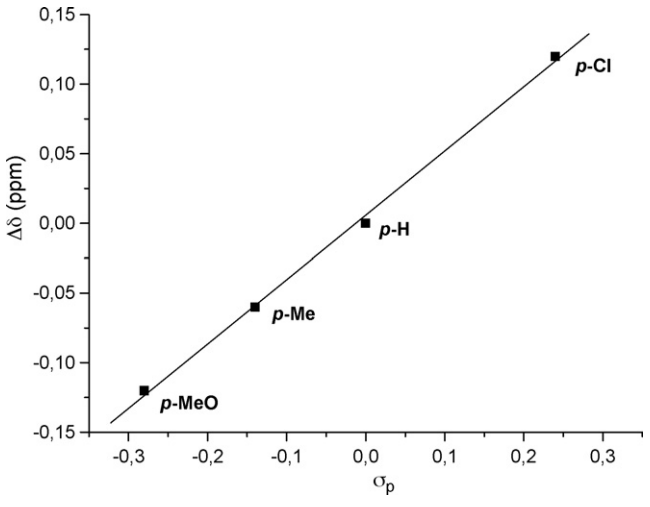

Fig. 3. Plot of the *N*–H ^{1}H NMR chemical shifts (ppm) *vs.* σ_p substituent parameters for complexes LII–LV. Reprinted with permission of Elsevier B.V. (Ref. [99]).

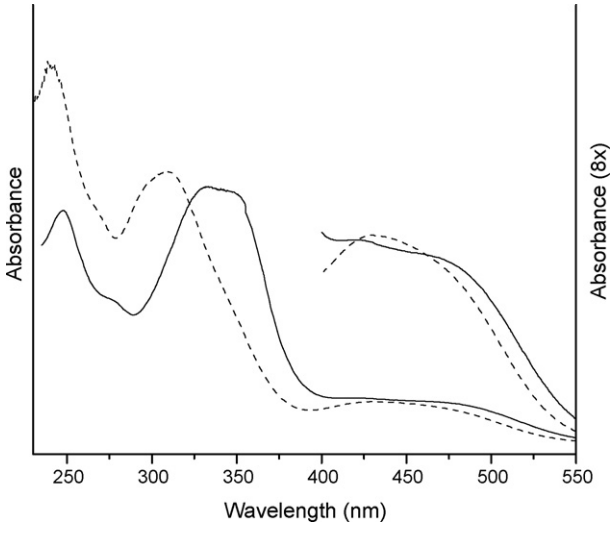

Fig. 4. UV–vis spectra of compounds **XLIX** (dashed line) and **LIV** (full line) demonstrating the effect of the conjugated bridge on absorption maxima [99].

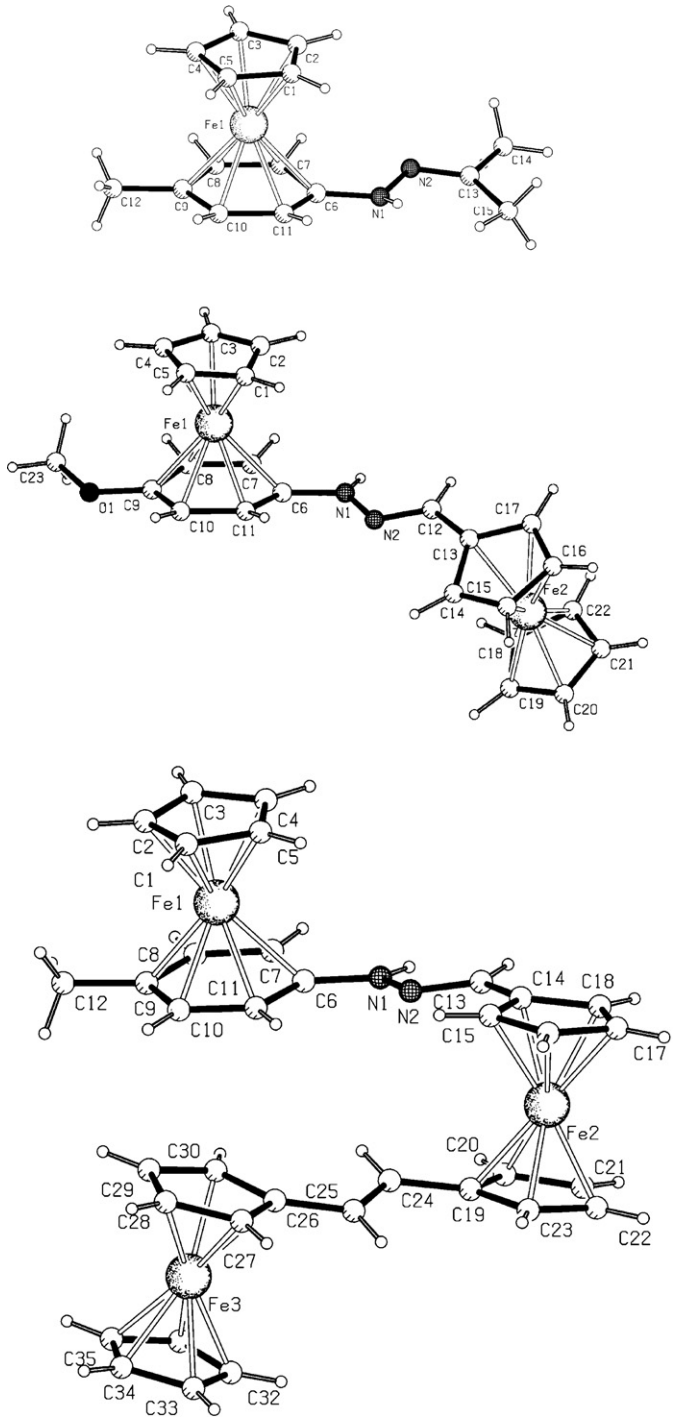

Fig. 5. Ball-and-stick views of $[(\eta^5\text{-Cp})Fe(\eta^6\text{-}C_6H_5\text{-}NHN{=}CMe_2)]^+$ [**X**]$^+$ (top [58]) $[(\eta^5\text{-Cp})Fe\{\eta^6\text{-}4\text{-}MeOC_6H_4\text{-}NHN{=}CH\text{-}(\eta^5\text{-}C_5H_4)Fe(\eta^5\text{-Cp})\}]^+$ [**XLVII**]$^+$ (middle [97]), and $[(\eta^5\text{-Cp})Fe\{\eta^6\text{-}4\text{-}MeC_6H_4\text{-}NHN{=}CH\text{-}(\eta^5\text{-}C_5H_4)Fe(\eta^5\text{-}C_5H_4)\text{-}CH{=}CH\text{-}(\eta^5\text{-}C_5H_4)Fe(\eta^5\text{-Cp})\}]^+$ [**LXXII**]$^+$ (bottom [102]). PF_6^- counterion has been omitted for clarity.

mixed-sandwich moieties adopt the same typical η^5-Fe-η^6 metallocene coordination mode. The carboxylic rings are essentially parallel with one another, with ring centroid-iron-ring centroid angles of 177.2–179.0°, and Fe–Cp and Fe-arene centroid distances of 1.640–1.675 and 1.544–1.580 Å, respectively. Similarly, we observe the concomitant lengthening of the Fe–C_{ipso} bond distances, ranging from 2.138 to 2.201 Å, and the shortening of the exocyclic C–N bond lengths (1.336–1.380 Å), leading to a slight iminium-cyclohexadienyl character of the coordinated C_6 ring with puckering angles of 3.10–10.3°. Those structural observations are common characteristics of hexahapto coordinated aromatic rings containing benzylic heteroatom [64–67] that have been theoretically rationalized by Saillard and co-workers [107]. Moreover, the conjugated hydrazonediyl transmitter backbone –N(R^2)–N=C(R^3)– displays a zigzag conformation with bond angles close to 120° at N(R^2), imine nitrogen and azomethine carbon atoms, respectively.

The most peculiar feature of the crystallographic study came out with the structure of the cationic binuclear derivative [**XLVIII**]$^+$ in which the R^3 substituent of the hydrazonediyl bridge is a methyl group. Indeed, the crystal structure shows the presence of both *syn*- and *anti*-rotamer, that is with the two iron atoms on the same and opposite faces of the dinucleating hydrazonato ligand, respectively, in the same asymmetric crystalline unit (Fig. 6) [59]. The *syn*/*anti* interconversion occurs by rotation of either the $[(\eta^5\text{-Cp})Fe(\eta^6\text{-}C_6H_5)\text{–}]^+$ fragment around the C_{phenyl}–N(R^2) bond, or of the ferrocenyl unit about its C_{ipso}–C(R^3) linkage, in line with both the presence of two ν(N–H) stretches in the solid state IR spectrum and the two rotational barriers observed in the variable-temperature NMR studies (see Section 3.2). In addition, theoretical investigations have shown that the two rotamers are close in energy, the *anti*-isomer being more stable than the *syn* one by only 0.12 eV [59]. To the best of our knowledge [**XLVIII**]$^+$ is the first bis-sandwich complex showing this peculiar arrangement in the solid state. For instance, the sterically less encumbered *anti*-isomer is the unique one found in the solid state for bis-$[(\eta^5\text{-Cp}')Fe]^+$ complexes of fulvalene [116,117] and polyarene [118,119]. This is also the case for all the structurally characterized binuclear (**XLVII**, **LVIII**, **LXV**) and trinuclear (**LXXII**) organometallic hydrazones with the unsubstituted spacer (R^3 = H). However, the symmetrical trimetallic hydrazone [**LXXI**]$^+$ escapes to this rule as it adopts the *syn* conformation with a Fe–Fe–Fe angle of 180° [101]. By contrast, only the *syn*-isomer occurs for [**LI**]$^+$ having the bulky *p*-tolyl substituent [98]. This unexpected behavior could presumably result from packing force effect in order to accommodate both sterically demanding *p*-tolyl and 1-ferrocenyl substituents at the azomethine carbon atom.

Several other structural peculiarities can be outlined. For instance, in the mononuclear series **XXI**, **XXV**, **XXXVIII**, **XXXIX** and **XLI**, the coordinated and free aromatic rings are virtually coplanar (dihedral angles ranging from 3.2° to 15.6°), thus creating a favorable orientation to the delocalization of the π-electron system along the entire hydrazone skeleton from the donor to the acceptor termini. It is also worth noting the "hinge-like" behavior of the 1,1′-ferrocenediyl subunit with the opening of the dihedral angle, made by the centroids of the coordinated C_6-ring, the two C_5H_4 rings and the remaining aromatic ring, from 21.3° for [**LXV**]$^+$ [101], to 53.9° for [**LXXII**]$^+$ [102] to 180° for [**LXXI**]$^+$ [101]. Finally, different kinds of hydrogen bond interactions were observed. So, the benzylic N–H group are involved in two types of hydrogen bonding: (i) intramolecularly with the oxygen atom of the *ortho*-methoxo-substituent (N···O separation of 2.627(4) Å) in compound [**XXI**]$^+$ [93], and (ii) in a strong interaction with a fluorine atom of the PF_6^- counter anion in both the binuclear **LVIII** [100] and trinuclear **LXXII** [102] derivatives with identical F···H separations of 2.20 Å. Moreover, in both complexes **LXXII** and **XXXIX** [95], the PF_6^- anion is also weakly coupled to the organometallic cation through hydrogen bond interactions between fluorine atoms and coordinated C–H aromatic groups, thus forming infinite zigzag chains in the latter case (Fig. 7). Complex **XXXIX** exhibits also a more surprising intramolecular hydrogen bond that implies an *ortho* C–H group of the coordinated C_6H_5 ring and the imine nitrogen atom, with C···N and H···N separations of 2.683 and 2.36 Å, respectively [95]. This results in the closure of the HC-C-N(Me)-N··· five-membered ring (Fig. 8).

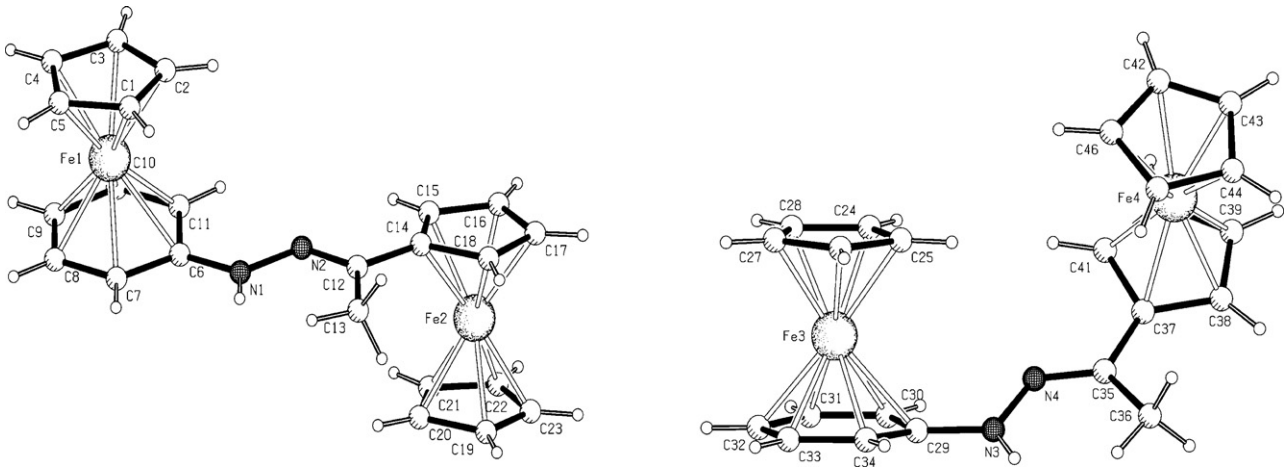

Fig. 6. Ball-and-stick views of *anti*-rotamer (left) and *syn*-rotamer (right) of $[(\eta^5\text{-Cp})Fe\{\eta^6\text{-}C_6H_5\text{-}NHN{=}C(Me)\text{-}(\eta^5\text{-}C_5H_4)Fe(\eta^5\text{-Cp})\}]^+$ [**XLVIII**]$^+$ [59]. PF_6^- counterions have been omitted for clarity.

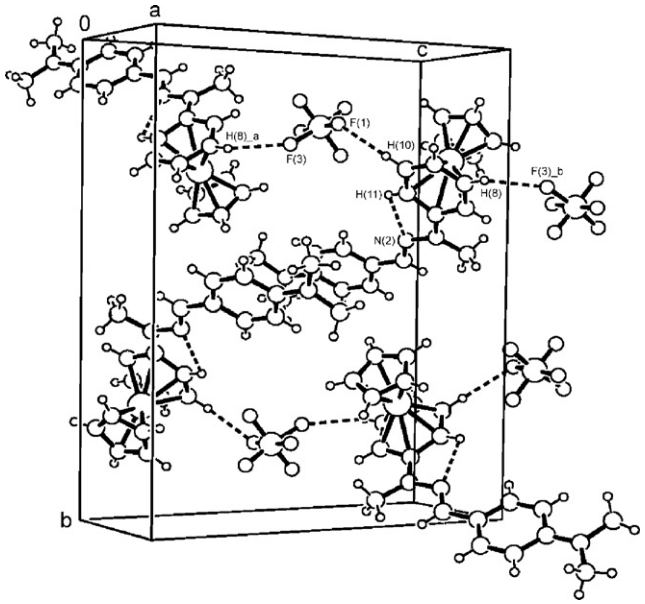

Fig. 7. Hydrogen bonding interactions in $[(\eta^5\text{-Cp})Fe\{\eta^6\text{-}C_6H_5\text{-}N(Me)N{=}CH\text{-}C_6H_4\text{-}4\text{-}NMe_2\}][PF_6]$, **XXXIX** [95].

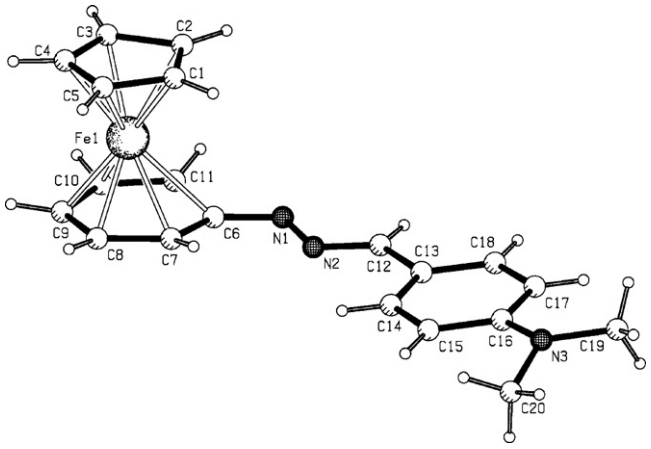

Fig. 8. Ball-and-stick view of the η^5-iminocyclohexadienyl/η^6-zwitterionic hybrid $[(\eta^5\text{-Cp})Fe(\eta^6\text{-}C_6H_5\text{-N-N}{=}CH\text{-}C_6H_4\text{-}4\text{-}NMe_2)]$ [106]. Solvating CH_2Cl_2 is omitted for clarity.

3.5. Reactivity

The activation of benzylic C–H bond in cationic arene-cyclopentadienyliron(II) complexes and subsequent bond formation of the resulting neutral cyclohexadienyl species with various elements is a well-established general and useful procedure for effecting modifications on the structure of the arene ligands [50–53]. This activation results from the enhancement of the acidity of the benzylic protons in the cationic complex [120]. Similarly, benzylic N–H activation also occurs at aminoarene ligand coordinated to the $[(\eta^5\text{-Cp})Fe]^+$ fragment to yield the corresponding imine complex, and subsequent treatment with an excess of alkylating reagents give rise to formation of new N–C bonds [121–124]. Accordingly, the *N*-methylated (R^2 = Me) hydrazone derivatives [**XXXVII**]$^+$, [**XXXVIII**]$^+$ and [**XXXIX**]$^+$, were synthesized from their respective unsubstituted (R^2 = H) precursors [**XXV**]$^+$, [**XXVI**]$^+$ and [**XXVII**]$^+$, in a one-pot two-step sequence (Scheme 2) [94]. The red zwitterionic intermediate is first generated at low temperature in dry tetrahydrofuran by deprotonating the benzylic N–H group with *n*-butyllithium, and then quenched with iodomethane to provide the final *N*-methylated organometallic hydrazones. They were isolated as air and thermally stable orange-red crystalline solids in yields ranging from 53 to 66%, and unambiguously characterized by ^{1}H NMR spectroscopy showing the appearance of a new singlet of the *N*-methyl proton resonance in the 3.53–3.73 ppm region. Moreover, complexes **XXXVIII** and **XXXIX** were authenticated by X-ray diffraction study [94,95]. Next, introduction of functional group following the $[(\eta^5\text{-Cp}')Fe]^+$-mediated benzylic deprotonation/alkylation sequence to such electroactive complexes would be of great interest in that, for instance, it could allow their transformation into precursors using covalent coupling, to obtain robust molecular arrays on a substrate.

Interestingly, the structure of the dark-red neutral intermediates is best described as a hybrid of η^5-iminocyclohexadienyl and η^6-zwitterionic hydrazonyl complexes. Indeed, the X-ray crystal structure analysis of the air and moisture sensitive complex $[(\eta^5\text{-Cp})Fe(\eta^6\text{-}C_6H_5\text{–N–N}{=}CH\text{–}C_6H_4\text{–4-}NMe_2)]$ (Fig. 8), isolated upon deprotonation of [**XXVII**]$^+$ with potassium *tert*-butoxide, shows a long Fe–C_{ipso} bond length of 2.303(13) Å and a doubly-bonded exocyclic C–N bond of 1.309(13) Å, resulting in a cyclohexadienyl folding angle of 12.5° [106]. This value is roughly two-fold greater than those measured for the cationic organometallic hydrazone species. In agreement with the X-ray data, the computed Fe–C_{ipso} Mülliken overlap population (+0.007 *vs.* +0.107 for the average value of the five other Fe–C bonds) suggests an almost

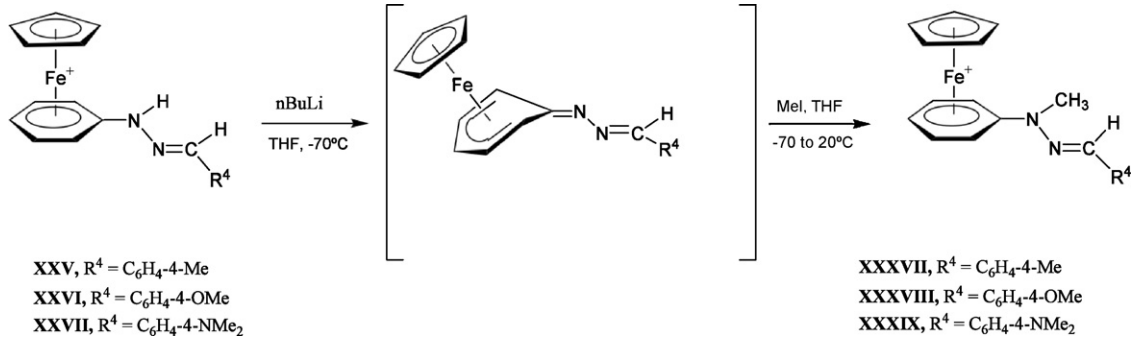

XXV, $R^4 = C_6H_4$-4-Me
XXVI, $R^4 = C_6H_4$-4-OMe
XXVII, $R^4 = C_6H_4$-4-NMe_2

XXXVII, $R^4 = C_6H_4$-4-Me
XXXVIII, $R^4 = C_6H_4$-4-OMe
XXXIX, $R^4 = C_6H_4$-4-NMe_2

Scheme 2. Synthesis of the cationic *N*-methylated mononuclear organometallic hydrazones [**XXXVII**]$^+$, [**XXXVIII**]$^+$ and [**XXXIX**]$^+$ (see Ref. [94]).

non-bonding interaction. The capacity change is also evidenced in solution by NMR spectroscopy. For instance, the ^{13}C signal of the *ipso* carbon shifts slightly downfield from 121.3 ppm in [**XXVII**]$^+$ to 128.9 ppm in the neutral compound. Such change supports a zwitterionic-type structure rather than a cyclohexadienyl one, for which a more downfield shift is expected. Astruc et al. reported on genuine cyclohexadienyl derivatives [(η^5-Cp)Fe(η^5-C_6Me_5=X)] (X = CH_2, NH, C=) for which the decoordinated carbon appears in the range 145–156 ppm [123,125,126]. The bonding situation we encountered with the neutral hydrazonyl complexes is, in fact, reminiscent of that observed by Johnson and Treichel for [(η^5-Cp)Fe(η-fluorenyl)] [127].

3.6. Electrochemical properties

The [(η^5-Cp)Fe(η^6-arene)]$^+$ complexes are well known for their interesting redox properties [128], the functions and applications of their reduced and oxidized forms [129], and their use for studying electronic communication between ligand-bridged metals [130]. As all the organometallic hydrazones depicted in Table 1 possess this redox active mixed-sandwich subunit, and in order to get a deeper insight into the mutual donor–acceptor interaction, we decided to examine the electronic influence of the various R^4 substituents (see Table 1) through the hydrazonediyl skeleton –N(R^2)–N=C(R^3)–, and of the methylation of the benzylic nitrogen as well as the azomethine carbon atoms, using electrochemistry. In particular, one can scrutinize these influences in terms of thermodynamics *via* the redox potentials and the stability of the 19-electron reduced redox state through the shapes of the cyclovoltammetry waves.

All the mono-, bi- and trinuclear hydrazones studied undergo a one-electron irreversible reduction process centered at the mixed-sandwich moiety, corresponding to the single-electron reduction of the $3d^6$, Fe^{II}, 18-electron complexes to the unstable $3d^7$, Fe^{I}, 19-electron species [128]. As well, the reduction potentials of the non *N*-methylated hydrazone derivatives (R^2 = H) are *ca.* 0.6 V more cathodic (Table 3) than those of their *N*-methylated analogues (R^2 = Me). This unexpected behavior arises from the reduction of the *in situ* generated neutral zwitterionic species (see the preceding Section), as it was checked by recording cyclic voltammograms of freshly prepared solutions of their deprotonated precursors [94]. Then, addition of iodomethane allows the recovery of the cyclovoltammograms of their corresponding cationic *N*-methylated hydrazone counterparts (Table 3). On the other hand, substitution of the 4-Me group for 4-OMe and 4-NMe_2 of the R^4 substituent in the three series of compounds **XXV**–**XXVII**, **XXXVII**–**XXXIX** and **XII**–**XIV** (Tables 3 and 4) causes a progressive displacement of the redox potentials of 40, 50 and 40 mV, respectively, toward more cathodic values (Me < MeO < NMe_2) [93,94]. This clearly indicates a significant electronic interaction between the electron donating and accepting termini through the –N(R^2)–N=CC(R^3)–C_6H_4– spacer, for these series of mononuclear hydrazones. One can also note that substitution at the azomethine carbon (R^3 = Me) rather than at the benzylic nitrogen (R^2 = Me) renders the reduction more difficult by 50–100 mV (Table 4). Finally, the cyclovoltammograms of the three organometallic hydrazones capped with the pentamethylcyclopentadienyl ligand, **XLIII**, **LXVI** and **LXVII** (Table 1) [60], present the same one-electron irreversible reduction process as their unsubstituted Cp counterparts, with redox potentials cathodically shifted by *ca.* 0.3 V. More interestingly, they also show a single-electron irreversible oxidation wave at 1.18, 1.23 and 1.51 V *vs.* Ag/AgCl (ferrocene as internal standard [131]), respectively (Fig. 9). Such a behavior has never been observed for any analogous organometallic hydrazones in the unsubstituted Cp series. The lowering of the oxidation potentials of **XLIII**, **LXVI** and **LXVII** thus, the observation of the oxidation waves, results from the permethylation of the cyclopentadienyl ring and its subsequent amplified donor capacity [107].

Besides the Fe^{II}/Fe^{I} redox process centered at the mixed-sandwich subunit, cyclovoltammograms of all the homobimetallic hydrazone complexes studied display also a reversible one-electron oxidation wave (Fig. 9). This anodic event is centered at the 1-ferrocenyl end group (**XLIV**–**LXIX** and **LXVI**) or at the 1,1′-ferrocenediyl spacer (**LX**–**LXV**), and corresponds to the generation of the dicationic Fe^{II}–Fe^{III} mixed valence species. In all the cases, the half-wave potentials ($E_{1/2}$) values of the reversible one-electron oxidations are positively shifted with respect to that of free ferrocene, thus illustrating the electron-withdrawing properties of the cationic [(η^5-Cp′)Fe(η^6-4-RC_6H_4-)]$^+$ entity. A more positive oxidation potential indicates that the ferrocenyl unit is more difficult to oxidize, *i.e.* less electron rich. This anodic difference ($\Delta E_{1/2}$) ranges from almost 0 for **LIV**, **LV** and **LVII** [99,100], to +221 mV

Table 3
Comparison (R^2 = H *vs.* R^2 = Me) of cyclic voltammetry data for related mononuclear compounds[a].

R^4	Compd. (R^2 = H)	E_{pc} (V)[b]	Compd. (R^2 = Me)	E_{pc} (V)[b]
C_6H_4-4-Me	**XXV**	−1.91	**XXXVII**	−1.35
C_6H_4-4-OMe	**XXVI**	−1.93	**XXXVIII**	−1.38
C_6H_4-4-NMe_2	**XXVII**	−1.95	**XXXIX**	−1.40

[a] Recorded in DMF at 298K with a vitreous carbon working electrode, 0.1 M *n*-$Bu_4^+PF_6^-$ as supporting electrolyte, scan rate 100 mVs^{-1}. All potentials are quoted *vs.* Ag/AgCl [131].
[b] Irreversible wave corresponding to the Fe^{II}/Fe^{I} couple.

Table 4
Comparison (R^2 = Me *vs.* R^3 = Me) of cyclic voltammetry data for related mononuclear compounds[a].

R^4	Compd. (R^2 = Me)	E_{pc} (V)[b]	Compd. (R^3 = Me)	E_{pc} (V)[b]
C_6H_4-4-Me	**XXXVII**	−1.38	**XII**	−1.48
C_6H_4-4-OMe	**XXXVIII**	−1.42	**XIII**	−1.50
C_6H_4-4-NMe_2	**XXXIX**	−1.47	**XIV**	−1.52

[a] Recorded in acetonitrile at 298 K with a vitreous carbon working electrode, 0.1 M *n*-$Bu_4^+PF_6^-$ as supporting electrolyte, scan rate 100 mV s^{-1}. All potentials are quoted *vs.* Ag/AgCl [131].
[b] Irreversible wave corresponding to the Fe^{II}/Fe^{I} couple.

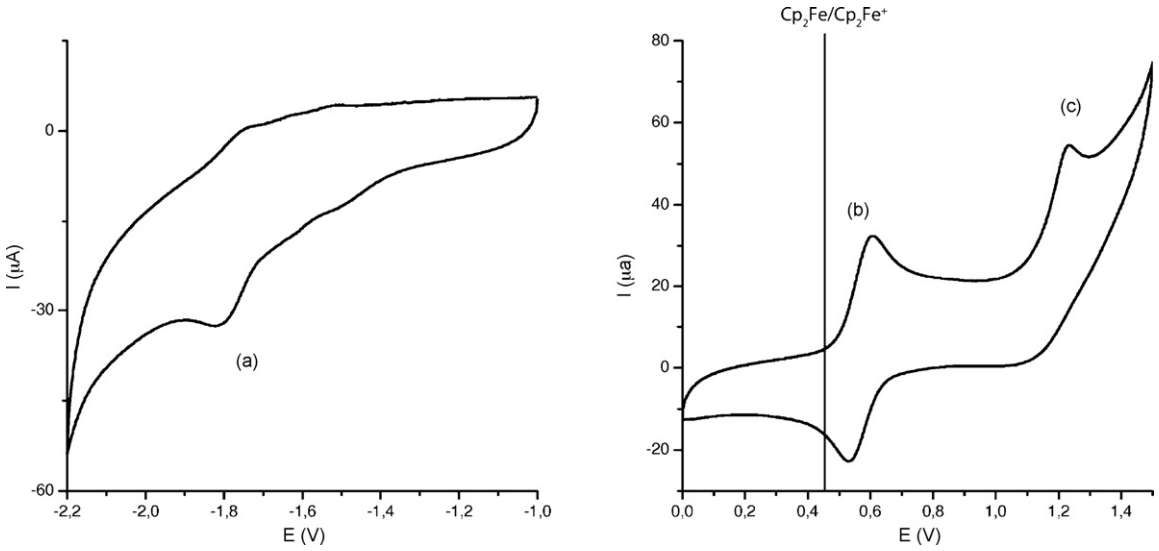

Fig. 9. Cyclic voltammograms of the homobimetallic hydrazone **LXVI** recorded in MeCN/0.1 M $nBu_4N^+PF_6^-$, T = 293 K, v = 0.1 V s^{-1}, reference electrode Ag/AgCl, internal reference $Cp_2Fe^{0/+}$ [131]. (a) Reduction of the $[(\eta^5\text{-Cp}^*)Fe(\eta^6\text{-}C_6H_5)]^+$ fragment; (b) oxidation and reduction of the 1-ferrocenyl unit; (c) oxidation of the $[(\eta^5\text{-Cp}^*)Fe(\eta^6\text{-}C_6H_5)]^+$ fragment.

for **LXIV** [101]. As expected, the greatest $\Delta E_{1/2}$ values are observed for the four bis-substituted complexes (**LX**–**LXIII**) with appended electron-withdrawing *para*-nitrostyril group. Compare for example, the $\Delta E_{1/2}$ values of complexes **XLIV** and **LX** in Table 5 where are listed the $\Delta E_{1/2}$ values of the six $[(\eta^5\text{-Cp}')Fe(\eta^6\text{-}C_6H_5)]^+$ containing binuclear hydrazones.

Two comments can be made from the data gathered in Table 5. First, despite the strong electron donating effect brought about by the five methyl substituents of the cyclopentadienyl ring in **LXVI**, the positive anodic shift is only 50 mV weaker than that measured for the parent homobimetallic complex **XLIV**, whereas substitution of the hydrazonediyl spacer at the azomethine carbon (R^3 = Me) in **XLVIII** has a greater impact as the $\Delta E_{1/2}$ drops by 70 mV. Second, comparison of the $\Delta E_{1/2}$ values of the four homobimetallic compounds **XLIV**, **XLVIII**, **LII** and **LVI**, in which the through-bond Fe···Fe distances range between 9.72 Å (**XLVIII** [59]) and 18.12 Å (**LVI** [100]), clearly shows that chain lengthening promotes a significant decrease in the oxidation potentials. These cathodic shifts, decreasing from 160 to 38 mV, might result from the stabilization of the positive charge of the oxidized species along the π-conjugated dinucleating ligand. These electrochemical findings are in perfect agreement with the electronic spectral data described in Section 3.3, with the gradual bathochromic shifts of the maximum of the high- and low-energy bands from 314 to 368 nm, and from 451 to 474 nm, respectively, on passing from the shortest (**XLIV**) to the longest (**LVI**) chromophores.

Table 5
$\Delta E_{1/2}$ *vs.* ferrocenium/ferrocene couple for $[(\eta^5\text{-Cp}')Fe(\eta^6\text{-}C_6H_5)]^+$ containing binuclear hydrazones[a].

Compound	$\Delta E_{1/2}$ (mV)	Compound	$\Delta E_{1/2}$ (mV)
XLIV	160	**LX**	176
XLVIII	90	**LII**	73
LXVI	110	**LVI**	38

[a] $\Delta E_{1/2} = E_{1/2}$(compound) − $E_{1/2}$(ferrocene), see also text.

The cyclovoltammograms of the symmetric homotrimetallic hydrazones (**LVIII**–**LXXI**) display the same two major features already observed for the binuclear counterparts: (i) an irreversible two-electron redox process assigned to Fe-centered reduction at the mixed-sandwich fragments, and (ii) a reversible single-electron oxidation wave corresponding to the bridging 1,1′-ferrocenediyl unit [101]. The largest $\Delta E_{1/2}$ value (225 mV) is measured for **LXIX**, presumably due to the enhanced electron-accepting nature of the cationic 4-chloro mixed-sandwich unit. On the other hand, two oxidation waves are observed for the trimetallic hydrazones **LXXII** and **LXXIII**, both having the 1-ferrocenyl and the 1,1′-ferrocenediyl connected by a *trans*-HC=CH linkage [102]. The first oxidation in each case corresponds to oxidation of the more electron-releasing terminal 1-ferrocenyl unit, and the second wave, the most anodic one, corresponds to the oxidation of the central 1,1′-ferrocenylene spacer. This cyclovoltammogram wave splitting suggests that there is some significant electronic communication between the iron centers of the ferrocenyl groups through the *trans*-ethenediyl core in these two complexes [132]. Thus, comproportionation constants Kc of 4075 and 7038 were computed for **LXXII** and **LXXIII**, respectively [102].

In summary, these electrochemical data suggest that the LUMO of all the organometallic hydrazones examined is determined by the cationic mixed-sandwich, and that the nature of the HOMO is dominated by the neutral donating ferrocenyl units, in accordance with theoretical investigations [59]. Moreover, the mutual electronic influence of electron donating and accepting termini is

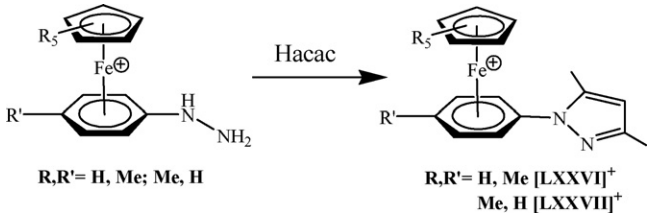

Scheme 3. Synthesis of the cationic organometallic pyrazoles [**LXXIV**]$^+$ and [**LXXV**]$^+$ (see Ref. [139]).

warranted by the hydrazonediyl spacer –N(R^2)–N=C(R^3)–, and as a result, they behave as donor-acceptor couples.

4. Organometallic pyrazoles

Pyrazoles [68] have been studied for over a century as an important class of heterocyclic compounds and still continue to attract considerable attention due to their wide range of biological, medicinal and anticancer activities [133,134]. In recent years, substantial effort has been devoted to the design and synthesis of new ferrocenyl-substituted pyrazole derivatives [135], with expectation of enhanced or unexpected biological activity which is absent or less manifest in the parent molecule [136–138]. In this context, having in hands the organometallic hydrazines depicted in Section 2, it was interesting to design new organometallic pyrazole derivatives in which the heterocyclic ring is bonded to the cationic organoiron mixed-sandwich fragment through a carbon–nitrogen linkage [139]. Moreover, the salt form of such compounds could be an important factor in terms of biological activity considering its solubility in water.

4.1. Synthesis and spectroscopy

The organoiron mixed-sandwich substituted 3,5-dimethylpyrazole complexes **LXXIV** and **LXXV** are straightforwardly synthesized by a 1:1 cyclocondensation reaction of 2,4-pentanedione with the corresponding organometallic hydrazines **II** and **VII**, respectively (Scheme 3). **LXXIV** and **LXXV** are air and thermally stable compounds that are isolated as red orange and yellow-orange analytically pure microcrystalline solid in 76 and 70% yields, respectively [138].

The spectroscopic properties of both compounds **LXXIV** and **LXXV** exhibit similar features indicating analogous molecular structures. For instance, in their solid (KBr) IR spectra the pyrazole stretches appear in the expected region at 1570–1480 cm^{-1}, in addition to the typical strong bands observed for the PF_6^- counter anion at 832 and 558 cm^{-1}. Their electronic spectra are characteristic of [(η^5-Cp′)Fe(η^6-arene)]$^+$ complexes, with the visible band responsible of their color centered at *ca.* 395 nm being broadened by overlapping with d–d transitions of the organometallic fragment [140,141]. Additionally, both **LXXIV** and **LXXV** give rise to the expected simple ^{1}H NMR spectra consisting, besides the classical resonances of the mixed-sandwich cores, of two well-separated singlets for the methyl substituents and one resonance for the CH_{pz} unit of the pyrazol-1-yl pendant group.

4.2. X-ray molecular structures

The structures of both complexes **LXXIV** and **LXXV** were also authenticated by single crystal X-ray diffraction analysis [139]. For the sake of comparison, ball-and-stick views of the cationic organometallic pyrazole entities [**LXXIV**]$^+$ and [**LXXV**]$^+$ are presented in similar perspectives in Fig. 10. As expected from spectroscopic data discussed above, both organometallic cations present similar structural parameters. The most noticeable difference lies in their molecular conformations. In fact, the phenyl and the pyrazol-1-yl rings are twisted about the exocyclic carbon–nitrogen bond, making a dihedral angle of 38.3(4)° and 25.3(7)°, respectively. Interestingly, both the carbon and nitrogen atoms are hybridized sp^2 but are connected through a single bond (d_{C-N} = 1.409(4) and 1.405(6) Å, respectively), which allows unrestrained rotation in solution. These C–N bond lengths are 0.1 Å larger than that measured for the deprotonated hydrazone complex (see Section 3.5).

Ferrocenylpyrazoles are known as versatile building blocks for hydrogen-bonded organometallic supramolecular assemblies [142], however, no such hydrogen bonds are observed in the crystalline packing of both our ionic organoiron pyrazoles. In contrast, as mentioned for several organometallic hydrazones in Section 3.4, we observe some weak C–H···F interactions [143], helping to the arrangement between the cationic mixed-sandwich units and the hexafluorophosphate ions in the crystal packing [144].

5. Organometallic–inorganic diazenido complexes

As stated in the Introduction of this review, much of the interest in transition-metal complexes containing organodiazenido ligands (NNR) [15–31] arises from their potential applications as models for intermediates in biological and industrial dinitrogen to ammonia conversion [32–35]. Even though different coordination modes have been observed, in the majority of mononuclear organodiazenido complexes, this ligand is η^1-bonded to transition-metal centers through the terminal N atom, giving a near linear M=N=NR fragment [30]. Mono- and *cis*-bis(organodiazenido) complexes are readily prepared by a "formal" condensation reaction [145,146] of monosubstituted hydrazines with *cis*-dioxo transition-metal coordination compounds [28]. In 1994, Hidai et al. reported on a novel μ-η^1:η^6-coordination mode of aryldiazenido bridge in heterobimetallic complexes of the type $L_nW(\mu\text{-}\eta^1\text{:}\eta^6\text{-N=N-C}_6H_4R)ML_n$ (M = Cr, Fe, Ru) that are obtained upon nucleophilic aromatic substitution of activated η^6-fluoroarene with anionic nitrogen- or neutral diazenido-tungsten compounds [64]. Interestingly, our organometallic hydrazines **I**–**VII** can also serve as building blocks in the construction of new inorganic–organometallic hybrid charge-transfer systems having the μ-η^1:η^6-aryldiazenido dinucleating ligand, upon condensation with *cis*-dioxomolybdenum species [147].

5.1. Synthesis

The heterodimetallic organodiazenido complexes of general formula [(η^5-Cp′)Fe(μ-η^6:η^1-4-RC_6H_4NN)Mo(η^2-$S_2CNEt_2)_3$]$^+PF_6^-$ (**LXXVI**–**LXXIX**) are prepared by reacting their respective organometallic hydrazine precursors [(η^5-Cp′)Fe(η^6-4-$RC_6H_4NHNH_2$)]$^+PF_6^-$ (**I**, **II**, **V** and **VII**) with $MoO_2(S_2CNEt_2)_2$ in the presence of one equivalent of sodium diethyldithiocarbamato trihydrate in refluxing methanol (Scheme 4). These heterobimetallic iron-molybdenum complexes are obtained as reddish-brown microcrystalline diamagnetic solids, consisting of organometallic and inorganic fragments bridged by an aryldiazenido ligand in a μ-η^6:η^1 fashion. As a result, the initial *cis*-dioxo molybdenum(VI) precursor is reduced to generate a molybdenum(IV) center adopting a pentagonal bipyramidal geometry. They were isolated in rather modest yields (23–34%) in the Cp series (**LXXVI**–**LXXVIII**), while complex **LXXIX** that contains the Cp* ligand was isolated in very good yield (82%). This presumably arises from an easier partial decoordination of [(η^5-Cp)Fe]$^+$ moiety than the bulkier and more electron rich [(η^5-Cp*)Fe]$^+$ in a common key intermediate along the reaction pathway.

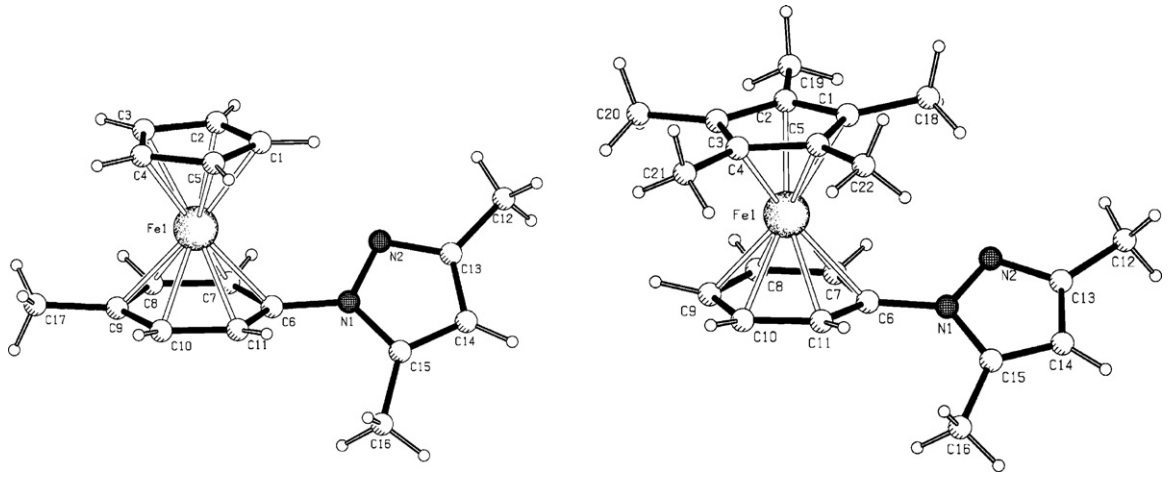

Fig. 10. Ball-and-stick views of cationic organometallic pyrazole complexes [**LXXIV**]$^+$ (left) and [**LXXV**]$^+$ (right) with the atom-labeling schemes [139].

Nevertheless, once formed, these four organometallic–inorganic hybrids are thermally stable (mp > 165 °C). In fact, their synthesis is invariably accompanied by the simultaneous formation of various amounts of green mononuclear organodiazenido compounds (η^1-4-RC_6H_4NN)Mo(η^2-$S_2CNEt_2)_3$, of which we structurally characterized the 4-methoxo derivative [147].

5.2. Spectroscopy

As major features of the solid (KBr) IR spectra of the three Cp-containing complexes **LXXVI**–**LXXIX** are the two characteristic prominent absorption bands of the ν(N=N) mode of the aryldiazenido or the ν(C···N) mode of the diethyldithiocarbamate ligands, in the 1506–1511 and 1433–1463 cm^{-1} regions [148,149]. The ν(N=N) stretching vibration for the Cp*-containing derivative **LXXIX**, splits into two identical strong and sharp bands at 1512 and 1500 cm^{-1}. Obviously, the spectra show also the two typical bands of the PF_6^- counter anion at *ca.* 840 and 558 cm^{-1}. On the other hand, the two most remarkable features observed in the ^{1}H NMR spectra come from, (i) the upfield shift of the Cp and Cp* proton resonances by ~0.2 ppm as the consequence of the attachment of the strong molybdenum *tris*-diethyldithiocarbamate electron-releasing fragment to the organoiron mixed-sandwich unit through the diazenido bridge, and (ii) the multiplicity pattern of the [Mo(η^2-$S_2CNEt_2)_3$]$^+$ proton resonances which consists in a triplet at *ca.* 1.20 ppm and a multiplet centered at *ca.* 1.25–1.30 ppm (methyl protons), and a second multiplet at *ca.* 3.85 ppm (methylene protons), with the 3:15:12 relative intensity. Such a splitting pattern ensues from a stereochemically rigid molecule bearing a plane of symmetry containing the molybdenum center, the diazenido fragment and one dithiocarbamate ligand with a sulfur atom in the apical position and the other one in the equatorial plane.

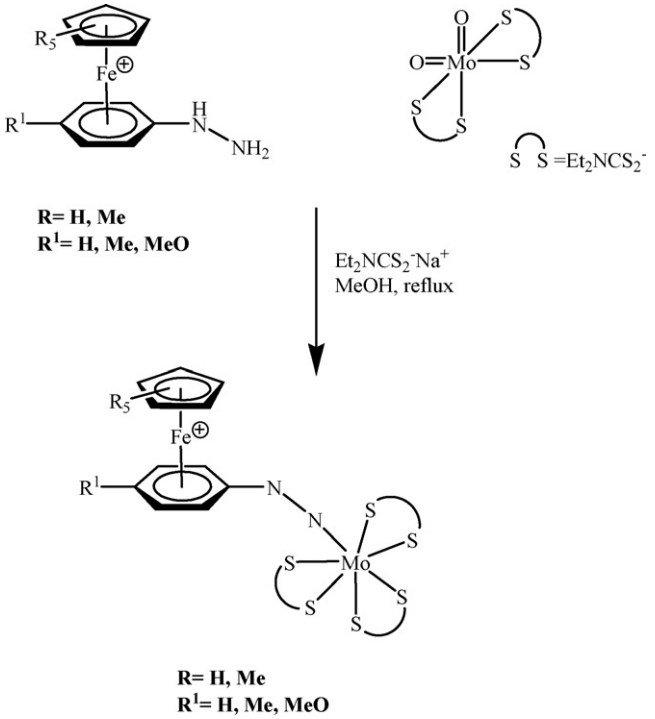

Scheme 4. Preparation of the cationic organometallic–inorganic diazenido complexes [**LXXVI**]$^+$–[**LXXIX**]$^+$ (see Ref. [147]).

The four iron–molybdenum complexes **LXXVI**–**LXXIX** exhibit similar UV–visible spectra, indicating similar structural features. Four types of absorption bands are observed: two in the UV region at 244–271 and 295–321 nm, and two others in the visible region, the first ones at 382–386 nm which are solvent independent and the second ones at 462–489 nm corresponding to a $Mo^{IV} \rightarrow Fe^{II}$ charge-transfer excitation through the aryldiazenido spacer [147]. The nature of this later band is ascertained by TD-DFT calculations (solvent effects not considered) performed on the structurally characterized (see below) complex **LXXVIII** [150]. The less energetic computed transition (736 nm), corresponding to transitions from the HOMO to the LUMO and LUMO + 1, can be assigned to the band observed at ~475 nm, thus confirming its Mo to Fe charge-transfer nature. A second computed transition at 669 nm with 60% weaker oscillator strength corresponds to mixed ligand/Mo charge-transfer to Fe, and likely contributes also to the band observed at ~475 nm. In addition, the absorption bands in the 462–489 nm range show a negative solvatochromism of 356–1148 cm^{-1} with increasing solvent polarity [151], *i.e.* on moving from CH_2Cl_2 (μ = 8.90) to DMSO (μ = 47.6) [152]. This trend, also observed in the case of the trimetallic hydrazones (see Section 3.3) [101], indicates a change in the dipole moment upon excitation from a more charge-localized ground state, with a high dipole moment, to an excited state where the positive charge is more delocalized throughout the entire molecule and the dipole moment is weaker [153].

5.3. Electrochemical behavior

Electrochemical potentials also offer information regarding donor–acceptor interactions, and we therefore explored, by

Table 6
Cyclic voltammetry data of the organometallic–inorganic hybrids **LXXVI** and **LXXIX**[a].

Compound	E_{pc} (V)[b]	$E_{1/2}$ (ΔE_p) [V (mV)][c]	E_{pa} (V)[d]
LXXVI	−1.89	0.41 (100)	1.12
LXXIX	−2.12	0.37 (110)	1.15

[a] Recorded in dichloromethane at 293 K with a Pt working electrode, with 0.1 M nBu$_4$N$^+$PF$_6^-$ as supporting electrolyte; all potentials are *vs.* $[(\eta^5\text{-Cp})_2\text{Fe}]^{0/+}$; scan rate = 0.1 V s^{-1}.
[b] Peak potential of the irreversible reduction wave Mo^{IV}/Mo^{III}.
[c] Peak-to-peak separation between the resolved reduction and oxidation wave maxima of the Mo^{IV}/Mo^{V} process.
[d] Estimated peak potential of the ill-resolved irreversible wave attributed to electrogenerated unstable trications.

cyclic voltammetry, the electronic influence of the acceptor $[(\eta^5\text{-Cp}')\text{Fe}]^+$ moiety on the donor $[\text{Mo}(\eta^2\text{-S}_2\text{CNEt}_2)_3]^+$ group through the phenyldiazenido linker, using the parent complex $[(\eta^5\text{-Cp})\text{Fe}(\mu\text{-}\eta^6\text{:}\eta^1\text{-C}_6\text{H}_5\text{-N=N})\text{Mo}(\eta^2\text{-S}_2\text{CNEt}_2)_3]^+$ [**LXXVI**]$^+$ and its pentamethylated cyclopentadienyl analogue [**LXXIX**]$^+$. The two compounds exhibit the same three redox events whose potentials are gathered in Table 6. Interestingly and contrary to our expectation based on previous observations in the organometallic hydrazone series (see Section 3.6), the irreversible wave observed under the cathodic regime corresponds to the one-electron reduction of the molybdenum(IV) center followed by a Mo–S bond cleavage, as found by DFT calculations [147]. The reversible redox system centered at 0.41 and 0.37 V for **LXXVI** and **LXXIX**, respectively, is confidently attributed to the 4d^2 Mo^{IV}/4d^1 Mo^{V} couple, according to our DFT calculations [147] and esr investigations on the mononuclear metal centered radical cation $[(\eta^1\text{-C}_6\text{H}_5\text{NN})\text{Mo}(\eta^2\text{-S}_2\text{CNMe}_2)_3]^+$ [154]. Moreover, the strong electronic cooperativity between the two metal centers is clearly evidenced by the large anodic shifts of 380 and 340 mV of the Mo^{IV}/Mo^{III} redox process of **LXXVI** and **LXXIX**, respectively, compared to that measured for the free mononuclear derivative $[(\eta^1\text{-C}_6\text{H}_5\text{NN})\text{Mo}(\eta^2\text{-S}_2\text{CNEt}_2)_3]$ [155].

In summary, these electrochemical data unambiguously confirm that the electron-withdrawing ability of the $[(\eta^5\text{-Cp})\text{Fe}]^+$ group is higher than that of $[(\eta^5\text{-Cp}^*)\text{Fe}]^+$ group as the reduction and oxidation potentials of complex [**LXXVI**]$^+$ are more anodic than those of complex [**LXXIX**]$^+$ [140]. These data also demonstrate that the nature of the HOMO is centered in the $[\text{Mo}(\eta^2\text{-S}_2\text{CNEt}_2)_3]^+$ moiety, whereas the character of the LUMO is determined by the cationic mixed sandwich $[(\eta^5\text{-Cp}')\text{Fe}(\eta^6\text{-C}_6\text{H}_5)]^+$, consistent with the electronic spectral data and Mo^{IV} → Fe^{II} charge-transfer transition through the phenyldiazenido ligand.

5.4. X-ray molecular structure

The crystalline and molecular structure of the ionic heterobimetallic diazenido complex $[(\eta^5\text{-Cp})\text{Fe}(\mu\text{-}\eta^6\text{:}\eta^1\text{-4-MeOC}_6\text{H}_4\text{NN})\text{Mo}(\eta^2\text{-S}_2\text{CNEt}_2)_3]^+\text{PF}_6^-$ (**LXXVIII**) was definitively established by X-ray diffraction study [147]. A ball-and-stick view of its cationic organometallic–inorganic hybrid entity is shown in Fig. 11. The crystal structure confirms the seven-coordinate pentagonal bipyramidal geometry of the molybdenum center, with two $[\eta^2\text{-S}_2\text{CNEt}_2]^-$ ligands in the equatorial plane and the third spanning an axial and an equatorial position, and the bridging coordination mode of the uninegatively charged aryldiazenido ligand [30]. This later occupies the remaining axial position through the terminal nitrogen atom with an almost linear Mo–N–N unit (171.5(6)°), while at the same time it is hexahapto coordinated to the $[(\eta^5\text{-Cp})\text{Fe}]^+$ moiety at a ring centroid-iron distance of 1.536 Å.

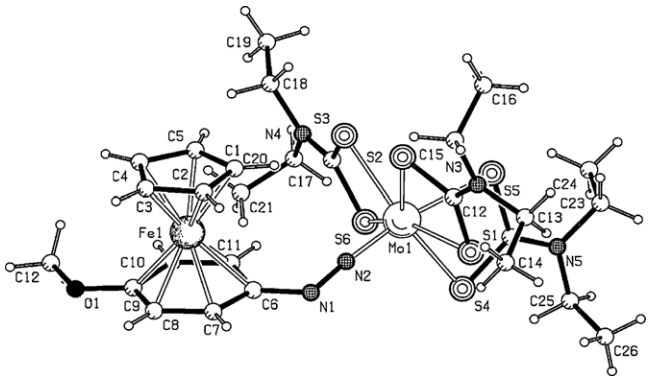

Fig. 11. Ball-and-stick view of the cationic organometallic–inorganic hybrid entity [**LXXVIII**]$^+$ with the atom-labelling scheme [147].

The mixed-sandwich unit presents the characteristic features we have already observed for all the structures depicted in this review. Those are a long Fe–C_{ipso} bond distance and a multiply bonded exocyclic C–N bond (see Table 7) giving rise to a dihedral folding angle (6.0(8)°) of the C_6-ring. As alluded in the introduction of Section 5, Hidai and co-workers have reported on similar heterobimetallic derivatives having the $\mu\text{-}\eta^6\text{:}\eta^1$-aryldiazenido bridging ligand [64]. In each of their compounds these authors observed also a lengthening of the metal–C_{ipso} bond and a shortening of the exocyclic C–N bond (Table 7). These observations were rationalized assuming that the aryldiazenido linker receives an important contribution of the zwitterionic resonance structure as a consequence of the presence of both the electron rich $[\text{W(dppe)}_2\text{X}]^+$ fragment (X = F, NCS) and the $[\text{ML}_n]^{0/+}$ electron-withdrawing arenophiles (M = Cr, Fe, Ru). Thus, the structure of complex [**LXXVIII**]$^+$ as well as that of its congeners is best described as a partially positively charged molybdenum center and a cyclohexadienyl-like character of the arene ring with a partial negative charge. As a result of this electron delocalization, the bonds of the Mo–N–N–C_{ipso} core of the heterobimetallic complexes lie somewhat between single- and double-bonds, whereas in mononuclear diazenido complexes lack-

Table 7
Comparison of selected bond lengths (Å) and bond angles (°) of heterobimetallic aryldiazenido cores and mononuclear related complexes.

Compound	Bond lengths (Å)			Bond angles (°)			Ref.
	M–C_{ipso}	C_{ipso}–N	N–N	N–M′	M′–N–N	N–N–C	
$[(\eta^5\text{-Cp})\text{Fe}(\mu\text{-}\eta^6\text{:}\eta^1\text{-4-MeOC}_6\text{H}_4\text{NN})\text{Mo}(\eta^2\text{-S}_2\text{CNEt}_2)_3]^+$ [**LXXVIII**]$^+$	2.140(7)	1.395(10)	1.276(9)	1.773(6)	171.5(6)	118.6(7)	[147]
$[(\eta^5\text{-Cp})\text{Fe}(\mu\text{-}\eta^6\text{:}\eta^1\text{-4-MeC}_6\text{H}_4\text{NN})\text{WF(dppe)}_2]^+$[a]	2.24(1)	1.35(1)	1.32(1)	1.778(8)	164.0(7)	120.6(8)	[64]
$[(\eta^5\text{-Cp})\text{Ru}(\mu\text{-}\eta^6\text{:}\eta^1\text{-C}_6\text{H}_5\text{NN})\text{W(NCS)(dppe)}_2]^+$[a]	2.39(2)	1.40(2)	1.28(1)	1.75(1)	166(1)	122(11)	[64]
$[(\text{OC})_3\text{Cr}(\mu\text{-}\eta^6\text{:}\eta^1\text{-4-MeO}_2\text{C-C}_6\text{H}_4\text{NN})\text{W(NCS)(dppe)}_2]$[a]	2.431(5)	1.366(6)	1.314(5)	1.784(4)	164.9(3)	120.0(4)	[64]
$[(\text{OC})_3\text{Cr}(\mu\text{-}\eta^6\text{:}\eta^1\text{-4-MeO}_2\text{C-C}_6\text{H}_4\text{NN})\text{WF(dppe)}_2]$[a]	2.50(1)	1.30(2)	1.33(2)	1.80(1)	161(1)	117(1)	[64]
$[(\eta^1\text{-4-MeC}_6\text{H}_4\text{NN})\text{Mo}(\text{-}\eta^2\text{-S}_2\text{CNEt}_2)_3]$	–	1.428(5)	1.234(5)	1.782(4)	170.4(3)	118.6(7)	[147]
$[(\eta^1\text{-C}_6\text{H}_5\text{NN})\text{Mo}(\eta^2\text{-S}_2\text{CNMe}_2)_3]$	–	1.417(7)	1.233(6)	1.781(4)	171.5(4)	120.5(5)	[156]
$[(\eta^1\text{-3-NO}_2\text{C}_6\text{H}_4\text{NN})\text{Mo}(\eta^2\text{-S}_2\text{CNMe}_2)_3]$	–	1.410(10)	1.262(9)	1.770(6)	170.6(6)	117.9(7)	[156]

[a] dppe = 1,2-bis-diphenylphosphinoethane.

ing the electron-withdrawing arenophile $[ML_n]^{0/+}$, the C_{ipso}–N and N–N bonds conserve their respective single- and double-bond character (Table 7) [20,23–25,27,30,31,156,157].

6. Conclusion and outlook

In this review, we have presented the synthesis, spectroscopic and structural characterization of a new family of air and thermally stable ionic organoiron mixed-sandwiches arylhydrazine complexes, and demonstrated their multifaceted synthetic abilities in the preparation of mono-, bi- and trinuclear hydrazones, and organometallic pyrazoles upon condensation reactions with a wide range of organic and organometallic carbonyl precursors. Indeed, π-coordination of the aromatic ring of organic arylhydrazines to the cationic $[(\eta^5\text{-Cp}')\text{Fe}]^+$ arenophile offers an exceptional opportunity to develop and increase the scope of their chemistry. Moreover, it has been shown that the organometallic hydrazines can also serve as building blocks in the construction of new inorganic–organometallic hybrid charge-transfer systems, in which the two metal centers are connected by the $\mu\text{-}\eta^1\text{:}\eta^6$-aryldiazenido dinucleating ligand, upon condensation with *cis*-dioxo molybdenum species. The original design of the new organometallic hydrazones combines the cationic mixed-sandwich acceptor $[(\eta^5\text{-Cp}')\text{Fe}(\eta^6\text{-aryl})]^+$, associated with an organic or organometallic donor through the asymmetric hydrazonediyl spacer, $-\text{N}(\text{R}^2)-\text{N}{=}\text{C}(\text{R}^3)-$. As such, these push–pull complexes can be defined as Type I non-rod-shaped dipolar chromophores [91,92], and have proved to favor electronic delocalization along the conjugated chain. These strongly polarised D-π-A systems exhibit solvatochromic properties, low-lying intramolecular charge transfer bands in their electronic absorption spectra and, for some of them, enhanced second-order NLO responses (μβ). Theoretical investigations are obviously required before discussing in more details the electronic structures of the complexes and the electronic transitions giving rise to the NLO properties. Such knowledge would allow further design and synthesis. A variety of transformations of an aromatic ligand subsequent to coordination to the strong electron-withdrawing $[(\eta^5\text{-Cp})\text{Fe}]^+$ activator reflect the powerful use of $[(\eta^5\text{-Cp})\text{Fe}]^+$-mediated arene syntheses [50–53]. In fact, the $[(\eta^5\text{-Cp})\text{Fe}]^+$ activation of arylhydrazones leads to clean benzylic N–H bond deprotonation to give thermally stable neutral complexes whose structures are intermediate between η^5-iminocyclohexadienyl and η^6-zwitterionic forms. Such hydrazonyl compounds that are unknown in organic chemistry are subsequently methylated. This N–H activation reaction is of great synthetic interest because it allows the formation of many N-element bonds by smooth reactions of a variety of electrophiles with the neutral deprotonated species. Functionalization of the neutral hydrazonyl species with organic moieties and substrates of biological interest may therefore be envisioned. Furthermore, all the work outlined here paved the way to a facile access to novel organometallic derivatives. There is no doubt that the π-complexed hydrazine building blocks can be engaged in other condensation reactions with carbonyl containing reagents to produce, for example, organometallic indoles or osazones.

Acknowledgements

We are grateful to Prof. J.-Y. Saillard and his co-workers (Rennes, theoretical investigations), and all the talented students and colleagues who have significantly contributed to the ideas and efforts involved in the work cited in this review. Financial support from the Fondo Nacional de Desarrollo Científico y Tecnológico, FONDECYT-Chile (Grants Nos. 1980433 and 1060490), the CONICYT, the CNRS, the Pontificia Universidad Católica de Valparaíso and the Université de Rennes 1 is gratefully acknowledged. The authors also acknowledge the Editor for helpful suggestions concerning electrochemistry.

References

[1] E. Fischer, Ber. Dtsch. Chem. Ges. 8 (1875) 589.
[2] For a historical overview of, E., Fischer's life, scientific accomplishment, see: H. Kunz, Angew. Chem. Int. Ed. 41 (2002) 4439.
[3] G.D. Byrkit, G.A. Michalek, Ind. Eng. Chem. 42 (1950) 1862.
[4] E.W. Schmidt, Hydrazine and its Derivatives: Preparation, Properties Applications, 1, 2nd ed., Wiley–Interscience, New York, 2001.
[5] B.T. Heaton, C. Jacob, P. Page, Coord. Chem. Rev. 154 (1996) 193.
[6] J. Chatt, A.J. Pearman, R.L. Richards, Nature 253 (1975) 39.
[7] C.E. Laplaza, C.C. Cummins, Science 268 (1995) 861.
[8] M.D. Fryzuk, J.B. Love, S.J. Rettig, V.G. Young, Science 275 (1997) 1445.
[9] Y. Nishibayashi, S. Iwai, M. Hidai, Science 279 (1998) 540.
[10] D.V. Yandulov, R.R. Schrock, Science 301 (2003) 76.
[11] J.A. Pool, E. Lobkovsky, P.J. Chirik, Nature 427 (2004) 527.
[12] L.D. Field, H.L. Li, S.J. Dalgarno, P. Turner, Chem. Commun. (2008) 1680.
[13] N.S. Lees, R.L. McNaughton, W.V. Gregory, P.L. Holland, B.M. Hoffman, J. Am. Chem. Soc. 130 (2008) 546.
[14] Y. Chen, Y. Zhou, P. Chen, Y. Tao, Y. Li, J. Qu, J. Am. Chem. Soc. 130 (2008) 15250.
[15] W.A. Nugent, B.L. Haymore, Coord. Chem. Rev. 31 (1980) 123.
[16] R.A. Henderson, G.J. Leigh, C.J. Pickett, Adv. Inorg. Chem. Radiochem. 27 (1983) 197.
[17] J.A. McCleverty, Transit. Met. Chem. 12 (1987) 283.
[18] B.F.G. Johnson, B.L. Haymore, J.R. Dilworth, in: G. Wilkinson, R.D. Gillard, J.A. McCleverty (Eds.), Comprehensive Coordination Chemistry, vol. 2, Pergamon, Oxford, 1987, p. 99.
[19] M.H. Chisholm, I.P. Rothwell, G. Wilkinson, R.D. Gillard, J.A. McCleverty (Eds.), Comprehensive Coordination Chemistry, vol. 2, Pergamon, Oxford, 1987, p. 161.
[20] W.A. Nugent, J.M. Mayer, Metal–Ligand Multiple Bonds, Wiley–Interscience, New York, 1988.
[21] K. Dehnicke, J. Sträle, Polyhedron 8 (1989) 707.
[22] K. Dehnicke, J. Sträle, Chem. Rev. 93 (1993) 981.
[23] D. Sutton, Chem. Rev. 93 (1993) 995.
[24] D.E. Wigley, Prog. Inorg. Chem. 42 (1994) 239.
[25] M. Hidai, Y. Mizobe, Chem. Rev., 95 (1995) 1115.
[26] D. Selmann, J. Sutter, Acc. Chem. Res. 30 (1997) 460.
[27] M. Hirsch-Kuchma, T. Nicholson, A. Davison, A.G. Jones, J. Chem. Soc. Dalton Trans. (1997) 3189.
[28] P. Gouzerh, A. Proust, Chem. Rev. 98 (1998) 77.
[29] For a reference gathering more than one hundred papers related to structurally characterized organohydrazido transition-metal complexes, see: S. Kahlal, J.-Y. Saillard, J.-R. Hamon, C. Manzur, D. Carrillo, J. Chem. Soc. Dalton Trans. (1998) 1229.
[30] For a reference gathering more than one hundred papers related to structurally characterized organodiazenido transition-metal complexes, see: S. Kahlal, J.-Y. Saillard, J.-R. Hamon, C. Manzur, D. Carrillo, New J. Chem. 25 (2001) 231.
[31] For a review on polynuclear molybdenum diazenido and hydrazido complexes, see: D. Carrillo, C. R. Chim. 3 (2000) 175.
[32] B.K. Burgess, D.J. Lowe, Chem. Rev. 96 (1996) 2983.
[33] J.B. Howard, D.C. Rees, Chem. Rev. 96 (1996) 2965.
[34] R.R. Eady, Chem. Rev. 96 (1996) 3013.
[35] V. Smil, Enriching the Earth: Fritz Haber, Carl Bosch and Transformation of World Food Production, MIT Press, Cambridge, MA, 2004.
[36] J. Chatt, J.R. Dilworth, R.L. Richards, Chem. Rev. 78 (1978) 590.
[37] M. Hidai, Y. Mizobe, Chem. Rev. 95 (1995) 1115.
[38] M. Hidai, Coord. Chem. Rev. 185–186 (1999) 99.
[39] M.D. Fryzuk, S.A. Johnson, Coord. Chem. Rev. 200–202 (2000) 379.
[40] B.A. MacKay, M.D. Fryzuk, Chem. Rev. 104 (2004) 385.
[41] M. Reiher, B. Kirchner, J. Hutter, D. Sellmann, B.A. Hess, Chem. Eur. J. 10 (2004) 4443.
[42] R.R. Schrock, Acc. Chem. Res. 38 (2005) 955.
[43] J.C. Peters, M.P. Mehn, in: W.B. Tolman (Ed.), Activation of Small Molecules, Wiley, Weinheim, 2006, p. 81.
[44] P.L. Holland, in: J.A. McCleverty, T.J. Meyer (Eds.), Comprehensive Coordination Chemistry II, vol. 8, Elsevier, Oxford, 2004, p. 569.
[45] G.J. Leigh, The World's Greatest Fix, Oxford University Press, Oxford, 2004.
[46] D. Astruc, Organometallic Chemistry and Catalysis, Springer, Berlin, 2007.
[47] D.A. Sweigart, J.A. Reingold, S.U. Son, in: R.H. Crabtree, D.M.P. Mingos (Eds.), Comprehensive Organometallic Chemistry III, vol. 5, Elsevier Science Ltd., Oxford, 2006, p. 761.
[48] E.P. Kündig (Ed.), Transition Metal Arene π-Complexes in Organic Synthesis and Catalysts, vol. 07, Top. Organomet. Chem., Springer, Berlin, 2004.

[49] F. Rose-Munch, E. Rose, in: D. Astruc (Ed.), Modern Arene Chemistry, Wiley-VCH, Weinheim, 2002, Chapter 11, p. 368.
[50] D. Astruc, S. Nlate, J. Ruiz, in: D. Astruc (Ed.), Modern Arene Chemistry, Wiley-VCH, Weinheim, 2002, Chapter 12, p. 400.
[51] A.S. Abd-El-Aziz, S. Bernardin, Coord. Chem. Rev. 203 (2000) 219.
[52] D. Astruc, Top. Curr. Chem. 160 (1991) 47.
[53] D. Astruc, Tetrahedron 39 (1983) 4027.
[54] A.F. Neto, J. Miller, An. Acad. Brasil Ciénc. 54 (1982) 331.
[55] A. Piórko, R.G. Sutherland, A. Vessières-Jaouen, G. Jaouen, J. Organomet. Chem. 512 (1996) 79.
[56] C.C. Lee, A.S. Abd-El-Aziz, R.L. Chowdhury, U.S. Gill, A. Piórko, R.G. Sutherland, J. Organomet. Chem. 315 (1986) 79.
[57] C. Manzur, L. Millán, M. Fuentealba, J.-R. Hamon, D. Carrillo, Tetrahedron Lett. 41 (2000) 3615.
[58] C. Manzur, E. Baeza, L. Millán, M. Fuentealba, P. Hamon, J.-R. Hamon, D. Boys, D. Carrillo, J. Organomet. Chem. 608 (2000) 126.
[59] C. Manzur, M. Fuentealba, L. Millán, F. Gajardo, D. Carrillo, J.A. Mata, S. Sinbandhit, P. Hamon, J.-R. Hamon, S. Kahlal, J.-Y. Saillard, New J. Chem. 26 (2002) 213.
[60] M. Fuentealba, L. Toupet, C. Manzur, D. Carrillo, I. Ledoux-Rak, J.-R. Hamon, J. Organomet. Chem. 692 (2007) 1099.
[61] C. Valério, E. Alonso, J. Ruiz, J.-C. Blais, D. Astruc, Angew. Chem. Int. Ed. 38 (1999) 1747.
[62] By comparison to a collection of structural data obtained through a Cambridge Data base search covering 60 $[(\eta^5\text{-Cp})Fe(\eta^6\text{-Arene})]^+$ compounds. Cambridge Data Base System, Cambridge Crystallographic Data Center, Version 5.12.
[63] A.G. Orpen, L. Brammer, F.H. Allen, D. Kennard, D.G. Watson, R. Taylor, J. Chem. Soc. Dalton Trans. (1989) S1.
[64] Y. Ishii, M. Kawaguchi, Y. Ishino, T. Aoki, M. Hidai, Organometallics 13 (1994) 5062.
[65] J.-Y. Saillard, D. Grandjean, P. Le Maux, G. Jaouen, Nouv. J. Chim. 5 (1981) 153.
[66] A.D. Hunter, L. Shilliday, W.S. Furey, M.J. Zaworotko, Organometallics 11 (1992) 1550.
[67] J.-P. Djukic, F. Rose-Munch, E. Rose, J. Vaissermann, Eur. J. Inorg. Chem. (2000) 1295.
[68] J. March, Advanced Organic Chemistry, 4th ed., Wiley–Intersciences, New York, 1992.
[69] L. Savini, L. Chiasserini, V. Travagli, C. Pellerano, E. Novellino, S. Cosentino, M.B. Pisano, Eur. J. Med. Chem. 39 (2004) 113.
[70] C.A.M. Fraga, E.J. Barreiro, Curr. Med. Chem. 13 (2006) 167.
[71] D.S. Kalinowski, D.R. Richardson, Pharmacol. Rev. 57 (2005) 547.
[72] D. Enders, L. Wortmann, R. Peters, Acc. Chem. Res. 33 (2000) 157.
[73] D. Enders, W. Bettray, in: S. Bräse, M. Christmann (Eds.), Asymmetric Synthesis – The Essentials, Wiley-VCH, Weinheim, 2006.
[74] T. Mino, Y. Shirae, T. Saito, M. Sakamoto, T. Fujita, J. Org. Chem. 71 (2006) 9499.
[75] T. Mino, K. Kajiwara, Y. Shirae, M. Sakamoto, T. Fujita, Synlett (2008) 2711.
[76] T.Z. Nagy, A. Csampai, A. Kotschy, Tetrahedron 61 (2005) 9767.
[77] A. Bermejo, A. Ros, R. Fernandez, J.M. Lassaletta, J. Am. Chem. Soc. 130 (2008) 15798.
[78] A.A.O. Sarhan, T. Izumi, J. Organomet. Chem. 675 (2003) 1.
[79] J. Silver, G.R. Fern, J.R. Miller, E. Slade, M. Ahmet, A. Houlton, D.J. Evans, G.J. Leigh, J. Organomet. Chem. 637–639 (2001) 311.
[80] C. López, J. Granell, J. Organomet. Chem. 555 (1998) 211.
[81] E.A. Raspopova, L.D. Popov, A.N. Morozov, I.N. Shcherbakov, V.A. Kogan, S.I. Levchenkov, Russ. J. Gen. Chem 78 (2008) 1586.
[82] M. Dartiguenave, J.M. Menu, E. Dyedier, Y. Dartiguenave, H. Siebald, Coord. Chem. Rev. 178–180 (1998) 623.
[83] T. Cantat, C.R. Graves, K.C. Jantunen, C.J. Burns, B.L. Scott, E.J. Schelter, D.E. Morris, P.J. Hay, J.L. Kiplinger, J. Am. Chem. Soc. 130 (2008) 17537.
[84] W.J. Evans, E. Montalvo, T.M. Champagne, J.W. Ziller, A.G. DiPasquale, A.L. Rheingold, Organometallics 27 (2008) 3582.
[85] S. Javed, D.M. Hoffman, Eur. J. Inorg. Chem. (2008) 5251.
[86] S. Javed, D.M. Hoffman, Inorg. Chem. 47 (2008) 11984.
[87] T. Hatakeyama, M. Nakamura, E. Nakamura, J. Am. Chem. Soc. 130 (2008) 15688.
[88] M. Ghedini, I. Aiello, A. Crispini, M. La Deda, Dalton Trans. (2004) 1386.
[89] J.J. Fernández, A. Fernández, M. López-Torres, D. Vázquez-García, A. Rodríguez, A. Varela, J.M. Vila, J. Organomet. Chem. 694 (2009) 2234.
[90] A. Fretzen, A. Ripa, R.G. Liu, G. Bernardinelli, E.P. Kündig, Chem. Eur. J. 4 (1998) 251.
[91] C. Serbutoviez, C. Bosshard, G. Knöpfle, P. Wyss, P. Pêtre, P. Günter, K. Schenk, E. Solari, G. Chapuis, Chem. Mater. 7 (1995) 1198.
[92] M.S. Wong, U. Meier, F. Pan, V. Gramlich, C. Bosshard, P. Günter, Adv. Mater. 8 (1996) 416.
[93] C. Manzur, L. Millán, W. Figueroa, J.-R. Hamon, J.A. Mata, D. Carrillo, Bol. Soc. Chil. Quím. 47 (2002) 431.
[94] C. Manzur, L. Millán, W. Figueroa, D. Boys, J.-R. Hamon, D. Carrillo, Organometallics 22 (2003) 153.
[95] W. Figueroa, M. Fuentealba, C. Manzur, D. Carrillo, J.A. Mata, J.-R. Hamon, J. Chil. Chem. Soc. 48 (2003) 75.
[96] L. Millán, M. Fuentealba, C. Manzur, D. Carrillo, N. Faux, B. Caro, F. Robin-Le Guen, S. Sinbandhit, I. Ledoux-Rak, J.-R. Hamon, Eur. J. Inorg. Chem. (2006) 1131.
[97] C. Manzur, M. Fuentealba, D. Carrillo, D. Boys, J.-R. Hamon, Bol. Soc. Chil. Quím. 46 (2001) 409.
[98] W. Figueroa, M. Fuentealba, C. Manzur, A.I. Vega, D. Carrillo, J.-R. Hamon, C. R. Chim. 8 (2005) 1268.
[99] A. Trujillo, M. Fuentealba, C. Manzur, D. Carrillo, J.-R. Hamon, J. Organomet. Chem. 681 (2003) 150.
[100] C. Manzur, M. Fuentealba, L. Millán, F. Gajardo, M.T. Garland, R. Baggio, J.A. Mata, J.-R. Hamon, D. Carrillo, J. Organomet. Chem. 660 (2002) 71.
[101] C. Manzur, C. Zúñiga, L. Millán, M. Fuentealba, J.A. Mata, J.-R. Hamon, D. Carrillo, New J. Chem. 28 (2004) 134.
[102] C. Manzur, L. Millán, M. Fuentealba, J.A. Mata, D. Carrillo, J.-R. Hamon, J. Organomet. Chem. 690 (2005) 1265.
[103] K. Nakamoto, Infrared and Raman Spectra of Inorganic and Coordination Compounds, 4th ed., John Wiley & Sons Inc., New York, 1986.
[104] C. Hansch, A. Leo, R.W. Taft, Chem. Rev. 91 (1991) 165.
[105] A.N. Nesmeyanov, I.F. Leshchova, Y.A. Ustynyuk, Y.I. Sirotkina, I.N. Bolesova, L.S. Isayeva, N.A. Vol'kenau, J. Organomet. Chem. 22 (1970) 689.
[106] W. Figueroa, M. Fuentealba, C. Manzur, D. Carrillo, A.I. Vega, J.-Y. Saillard, J.-R. Hamon, Organometallics 23 (2004) 2515.
[107] J. Ruiz, F. Ogliaro, J.-Y. Saillard, J.-F. Halet, F. Varret, D. Astruc, J. Am. Chem. Soc. 120 (1998) 11693.
[108] S. Barlow, S.R. Marder, Chem. Commun. (2000) 1555.
[109] J. Heck, S. Dabek, T. Meyer-Friedrichsen, H. Wong, Coord. Chem. Rev. 190–192 (1999) 1217.
[110] J.A. Mata, E. Falomir, R. Llusar, E. Peris, J. Organomet. Chem. 616 (2000) 80.
[111] R.P. Hsung, C.E.D. Chidsey, L.R. Sita, Organometallics 14 (1995) 4808.
[112] A.S. Abd-El-Aziz, T.H. Afifi, W.R. Budakowski, K.J. Friesen, E.K. Todd, Macromolecules 35 (2002) 8929.
[113] E. Peris, Coord. Chem. Rev. 248 (2004) 279.
[114] J. Zyss, I. Ledoux, J.-F. Nicoud, in: D.S. Chemla, J. Zyss (Eds.), Macromolecular Nonlinear Optics, Academic Press, San Diego, 1994, p. 129.
[115] C. Lambert, W. Gaschler, M. Zabel, R. Matschiner, R. Wortmann, J. Organomet. Chem. 592 (1999) 109.
[116] M.-H. Delville, F. Robert, P. Gouzerh, J. Linares, K. Boukheddaden, F. Varret, D. Astruc, J. Organomet. Chem. 451 (1993) C10.
[117] S. Rittinger, D. Buchholz, M.-H. Delville-Desbois, J. Linarès, F. Varret, R. Boese, L. Zolnai, G. Huttner, D. Astruc, Organometallics 11 (1992) 1454.
[118] M. Lacoste, F. Varret, L. Toupet, D. Astruc, J. Am. Chem. Soc. 109 (1987) 6504.
[119] D. Astruc, M. Lacoste, L. Toupet, J. Chem. Soc. Chem. Commun. (1990) 558.
[120] H. Trujillo, C.M. Casado, J. Ruiz, D. Astruc, J. Am. Chem. Soc. 121 (1999) 5674.
[121] J.F. Helling, W.A. Hendrickson, J. Organomet. Chem. 168 (1979) 87.
[122] C.C. Lee, U.S. Gill, R.G. Sutherland, J. Organomet. Chem. 206 (1981) 89.
[123] P. Michaud, D. Astruc, J. Chem. Soc. Chem. Commun. (1982) 416.
[124] C. Moinet, E. Raoult, J. Organomet. Chem. 231 (1982) 245.
[125] D. Astruc, J.-R. Hamon, E. Roman, P. Michaud, J. Am. Chem. Soc. 103 (1981) 7502.
[126] C.M. Casado, T. Wagner, D. Astruc, J. Organomet. Chem. 502 (1995) 143.
[127] J.W. Johnson, P.M. Treichel, J. Am. Chem. Soc. 99 (1977) 1427.
[128] D. Astruc, Chem. Rev. 88 (1988) 1189;
D. Astruc, Electron Transfer and Radical Reactions in Transition-Metal Chemistry, VCH, New York, 1995, Chapter 2, pp. 147–149.
[129] D. Astruc, New J. Chem. 33 (2009) 1191.
[130] D. Astruc, Acc. Chem. Res. 30 (1997) 383.
[131] For accepted values for ferrocene correction to SCE in many solvents, see: N.G. Connelly, W.E. Geiger, Chem. Rev. 96 (1996) 877.
[132] J.-P. Launay, Chem. Soc. Rev. 30 (2001) 386, and references cited therein.
[133] J. Elguero, in: A.R. Katritzky, C.W. Rees, E.F.V. Scriven (Eds.), Comprehensive Heterocyclic Chemistry II, vol. 3, Pergamon Press, Oxford, 1996, p. 1.
[134] C. Lamberth, Heterocycles 71 (2007) 1467.
[135] M. Zora, A. Nur Pinar, M. Odabaşoğlu, O. Büyükgüngör, G. Turgut, J. Organomet. Chem. 693 (2008) 145, and references cited therein.
[136] G. Jaouen (Ed.), Bioorganometallics: Biomolecules, Labeling Medicine, Wiley, Weinheim, 2006.
[137] N. Metzler-Nolte, M. Salmain, in: P. Štěpnička (Ed.), Ferrocenes, Wiley, Weinheim, 2008, Chapter 13, p. 499.
[138] D.R. van Staveren, N. Metzler-Nolte, Chem. Rev. 104 (2004) 5931.
[139] C. Manzur, L. Millán, M. Fuentealba, A. Trujillo, D. Carrillo, J. Organomet. Chem. 694 (2009) 2043.
[140] J.-R. Hamon, D. Astruc, P. Michaud, J. Am. Chem. Soc. 103 (1981) 758.
[141] W.H. Morrison, E.Y. Ho, D.N. Hendrickson, Inorg. Chem. 14 (1975) 500.
[142] M. Tomoyuki, S. Fumiko, S. Hirotaka, O. Kazuya, S. Fuminori, K. Daisuke, J. Organomet. Chem. 692 (2007) 1834.
[143] G.R. Desiraju, T. Steiner, The Weak Hydrogen Bond, Oxford University Press, Inc., New York, 1999.
[144] D. Braga, F. Grepioni, G.R. Desiraju, Chem. Rev. 98 (1998) 1375.
[145] T.-C. Hsieh, J.A. Zubieta, Polyhedron 5 (1986) 305.
[146] T.-C. Hsieh, S.N. Shaikh, J. Zubieta, Inorg. Chem. 26 (1987) 4079.
[147] C. Manzur, L. Millán, M. Fuentealba, J.-R. Hamon, L. Toupet, S. Kahlal, J.-Y. Saillard, D. Carrillo, Inorg. Chem. 46 (2007) 1123.
[148] M.W. Bishop, G. Butler, J. Chatt, J.R. Dilworth, G.J. Leigh, J. Chem. Soc. Dalton Trans. (1979) 1843.
[149] J.R. Dilworth, J.R. Miller, J. Chem. Educ. 68 (1991) 788.
[150] DFT calculations were carried out on a simplified model of $[LXXVIII]^+$ in which the ethyl groups of the diethyldithiocarbamato ligands are replaced by hydrogen atoms. The model complex IS labelled $[LXXVIII]^+$.

[151] A.B.P. Lever, Inorganic Electronic Spectroscopy, 2nd ed., Elsevier, Amsterdam, 1984, pp. 208–212.
[152] C. Reichardt, Chem. Rev. 94 (1994) 2319.
[153] E.S. Dodsworth, M. Hasegawa, M. Bridge, W. Linert, in: A.B.P. Lever (Ed.), Comprehensive Coordination Chemistry II: From Biology to Nanotechnology, vol. 2, Elsevier, New York, 2003, pp. 351–365.
[154] G. Butler, J. Chatt, G.J. Leigh, C.J. Pickett, J. Chem. Soc. Dalton Trans. (1979) 113.
[155] J.R. Dilworth, B.D. Neaves, C.J. Pickett, Inorg. Chem. 19 (1980) 2859.
[156] G. Butler, J. Chatt, G.J. Leigh, A.R.P. Smith, G.A. Williams, Inorg. Chim. Acta 28 (1978) L165.
[157] M. Hidai, Y. Mizobe, Can. J. Chem. 83 (2005) 358.